ASTEC-AP-2020-001 v1.1

19 July 2021
lee.jones@stfc.ac.uk

Report on the Performance Characterisation of Caesium Telluride and Caesium Potassium Antimonide Photocathodes Manufactured at CERN

L.B. Jones & T.C.Q. Noakes
Accelerator Science and Technology Centre
STFC Daresbury Laboratory
Warrington WA4 4AD, United Kingdom

D.P. Juarez–Lopez & L.A.J. Soomary
Department of Physics, University of Liverpool
Liverpool L69 7ZE, United Kingdom

H. Panuganti, E. Chevallay & V. Fedosseev
The European Organization for Nuclear Research (CERN)
1211 Geneva 23, Switzerland

Keywords: CsTe, CsKSb, photocathode, TESS, energy spread, TEDC

Summary

An analysis of four alkali and bi–alkali photocathodes grown at CERN was carried out at the STFC Daresbury Laboratory. The analysis involved measurements of surface composition via X–ray Photoelectron Spectroscopy (XPS), surface roughness via in–vacuum Scanning Tunnelling Microscopy (STM) and the Mean Transverse Energy (MTE) for each photocathode. Transverse Energy Distribution Curves (TEDC) were measured for each Cs–Te alkali metal photocathode at room and cryogenic temperatures and at room temperature for the Cs–K–Sb bi–alkali photocathode, and MTE extracted from this data.

A further experiment was carried out to investigate photoemission from Cs–Te photocathodes at visible wavelengths which involved the ceasiation of an additional polycrystalline copper photocathode puck from the same batch as those used as substrates for the original photocathode growth at CERN.

Contents

1 Introduction

In a collaboration between the STFC Daresbury Laboratory and CERN, Caesium Telluride alkali metal (Cs–Te) and Caesium Potassium Antimonide bi–alkali (Cs–K–Sb) photocathodes[1] were manufactured at CERN using the CLIC/CTF3 preparation facility [Chevallay et al., 2012]. These photocathodes were then transported overland to the STFC Daresbury Laboratory inside an Ultra–High Vacuum (UHV) suitcase which maintained a base pressure of $< 1\,\mathrm{E}^{-10}$ mbar for the 24 hour duration of the journey. This vacuum level was maintained during the unloading of the photocathodes and their transfer into the test facilities at Daresbury.

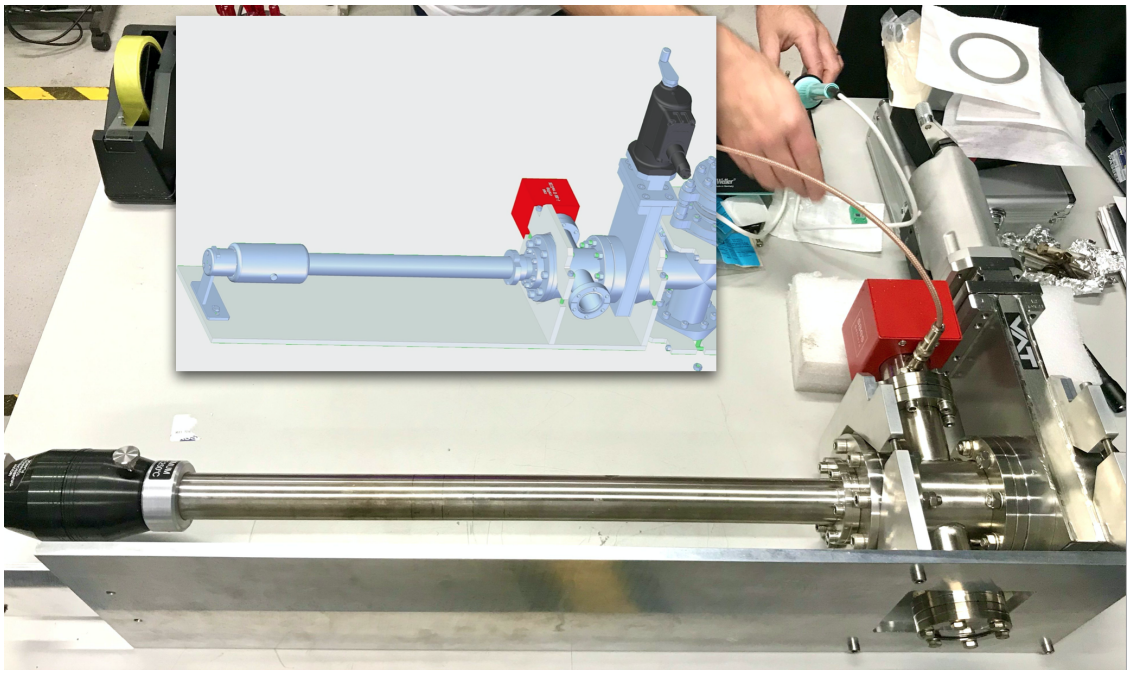

Figure 1: Photograph and schematic inset of the vacuum suitcase. Note that the schematic inset shows the valve orientated perpendicular to the ion pump, while the assembled version has the valve orientated parallel to the ion pump.

Figure 1 shows the vacuum suitcase as it arrived in the VISTA[2] laboratory at Daresbury on January 28$^{\text{th}}$ 2020 with the 4 photocathodes inside. UHV conditions were maintained during transportation through a combination of non–evaporable getter (NEG) and ion pumping, using a *FerroVac LSA2.1* battery–driven high voltage power supply to continuously drive the ion pump during transportation.

Four cathodes were manufactured at CERN, labelled Cathode P1, P2, P3 and P4 respectively, their assignment relating only to their position inside the vacuum suitcase during their transfer to Daresbury. P1, P2 and P4 are alkali metal photocathodes based on caesium telluride (Cs–Te), while P3 is a bi–alkali caesium potassium antimonide (Cs–K–

[1] A stoichiometrically–independent representation has been used in chemical formulae to avoid any specific reference to the ratio of the constituent elements.

[2] Vacuum Interfaces and Surface Technologies for Accelerators

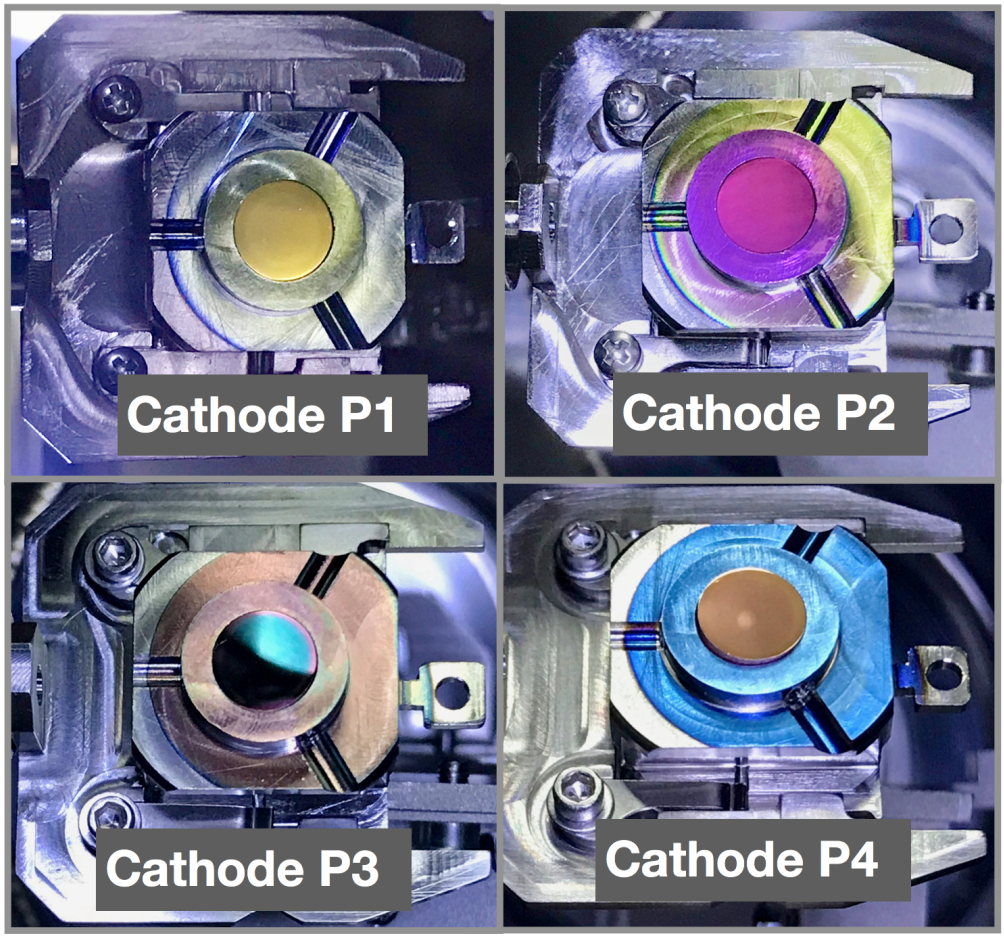

Figure 2: Photographs showing the photocathodes manufactured at CERN. P1, P2 and P4 are Cs–Te and P3 is a Cs–K–Sb. The photographs were taken in the TESS experimental system, through the same viewport and under the same lighting conditions as each photocathode was sequentially unloaded from the vacuum suitcase.

Sb). The photocathodes were grown on copper polycrystalline pucks supplied by SPL[3] using high–purity OFHC copper bar sourced from Advent Materials. All are shown in Figure 2, and it can be seen that there is a high degree of variability in the as–grown photocathodes indicated by the range of surface colouration.

The photocathode surfaces were characterised using the SAPI *Multiprobe* instrument [Noakes et al., 2014], and their photoemission performance characteristics were measured using the TESS [Jones et al., 2013]. Surface characterisation and photoemission performance data are presented for some of these Cs–Te and Cs–K–Sb photocathodes including surface composition via XPS, surface roughness via in–vacuum STM, quantum efficiency (QE) and the Mean Transverse Energy (MTE) extracted from their Transverse Energy Distribution Curve (TEDC) as a function of illumination wavelength.

[3]Surface Preparation Laboratory, Penningweg 69F, 1507 DE Zaandam, The Netherlands.

2 Bi–alkali photocathode growth method

Photocathode growth was performed by Eric Chevallay and Harsha Panguanti at CERN using the CLIC/CTF3 preparation facility [Chevallay et al., 2012]. One photocathode was grown each day over a 4 day period, with STFC staff present only for 2 of the 4 growths, hence the limited information on the details of the growth procedure. At the time of photocathode deposition, CERN were partway through an upgrade to their photocathode growth system. As such, their data logging facilities had been substantially upgraded so it was possible to capture all details relating to photocathode growth, but the actual control system had not been upgraded. Consequently control of the deposition process was manual for both the Cs–Te and Cs–K–Sb photocathodes, leading to a reduction in consistency and increased scope for operator error.

The co–deposition synthesis for photocathode P3 started with the heating of the substrate to 140 °C, followed by Sb deposition of several nanometers. The potassium dispenser was then exposed and K vapour was then co–deposited on the already established Sb film with continued Sb deposition. The target rate for K deposition was 0.1 nm/min.

Once a quantum efficiency (QE) response was seen from the Sb and K co–layer, Cs deposition commenced. From this point forward, all the three primary elements in the photoemissive film are being deposited simultaneously. The evaporation rate of a given element was controlled manually by the operator through minute adjustments of the current driving the corresponding dispenser.

The deposition rates and durations were adjusted while monitoring and maximising the measured photocurrent in real time, with adjustments based on previous experience. During the deposition process, the pressure in the preparation chamber reached 3.2×10^{-7} mbar.

3 XPS Surface composition analysis

The equipment used for the following analysis consists of a PSP model CTX400 X–ray source using an Al filament for K_α emission at 1,487 eV combined with a Thermo Scientific Alpha 110 hemispheric electron energy analyser.

3.1 P1 Cs-Te photocathode XPS

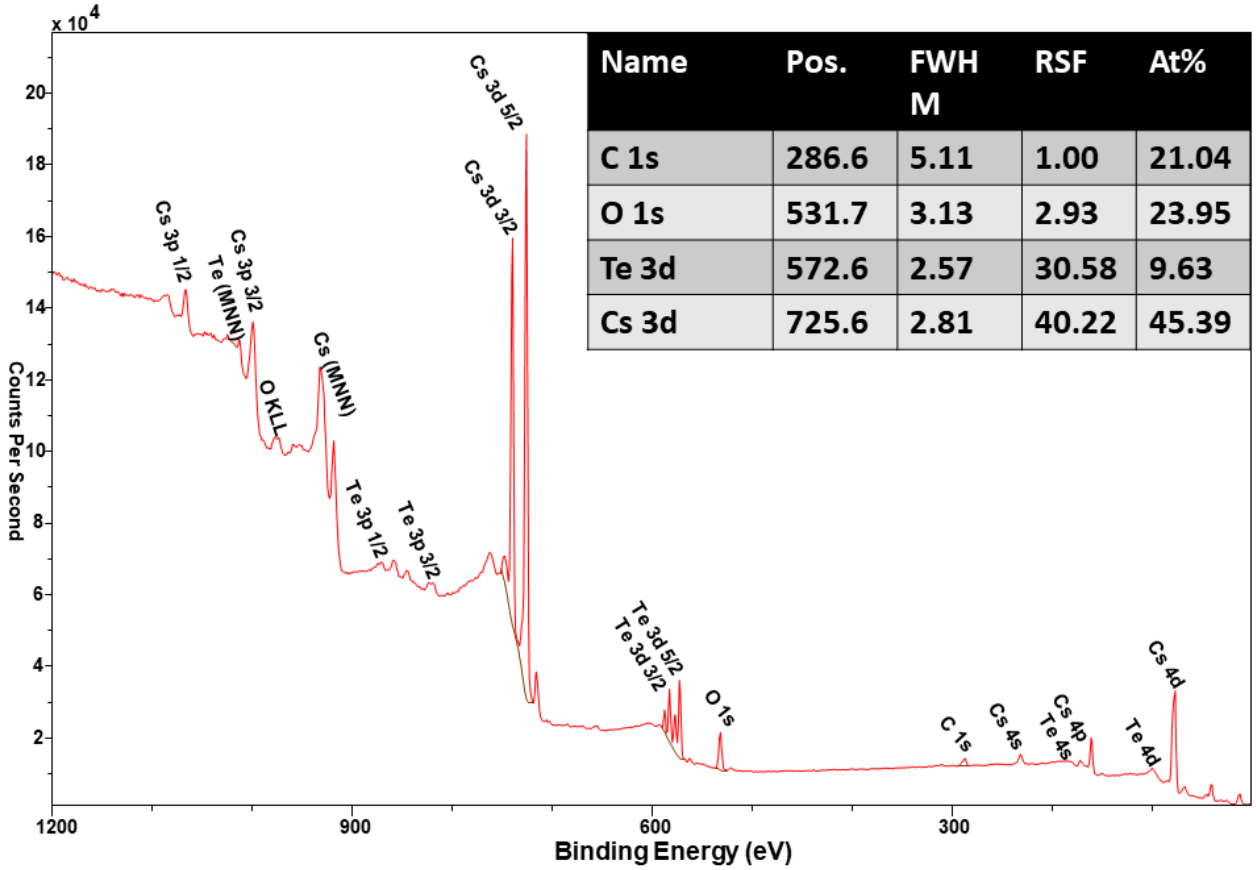

Name	Pos.	FWHM	RSF	At%
C 1s	286.6	5.11	1.00	21.04
O 1s	531.7	3.13	2.93	23.95
Te 3d	572.6	2.57	30.58	9.63
Cs 3d	725.6	2.81	40.22	45.39

Figure 3: Full–range XPS survey spectrum with preliminary peak assignments for the P1 Cs–Te photocathode.

Figures 3 and 4 show the survey scan for the P1 Cs–Te cathode, with the inset detailing specific components of interest. The major peaks for the elements detected are assigned, including the states originating from Cs, Te, O and C with spin–orbit splitting of p and d electrons noted. This data was recorded after the photocathode was transferred from the TESS to the Multiprobe system using a vacuum suitcase, and so does not reflect the chemical state of the photocathode when it was first received at Daresbury.

As can be seen in Figure 4, there is a significant level of oxidation on the surface. The carbon contamination at 286.6 eV, while not as high as that found for the P3 Cs–K–Sb cathode, was measured at 21.0 % of the contribution. The atomic percentage of Cs, Te and O are reported as 45.4 %, 9.6 % and 24.0 % respectively, as can be seen in Table 1.

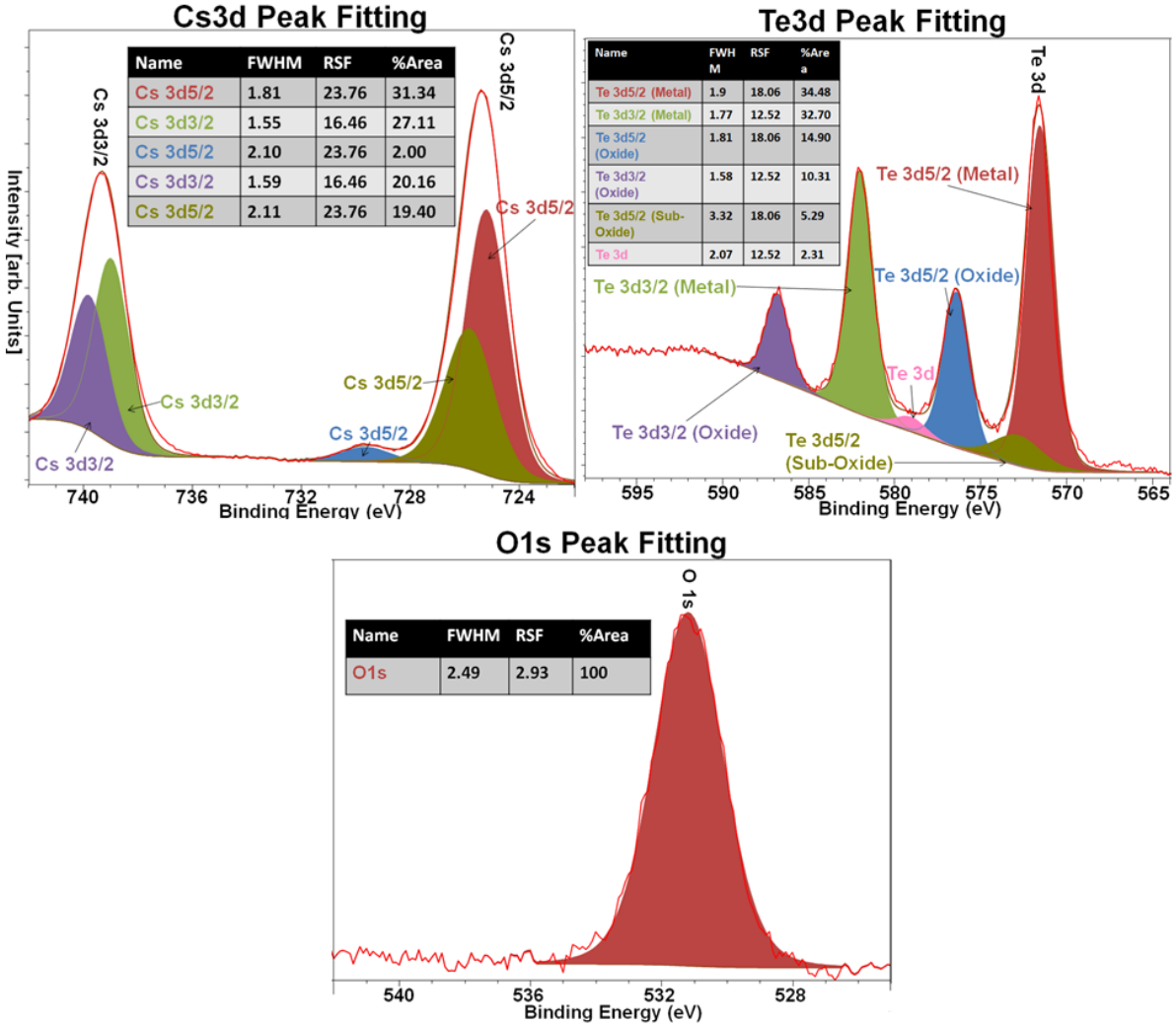

Figure 4: Peak fitting for the P1 Cs–Te cathode. The XPS data was taken after transfer by vacuum suitcase from the TESS to our surface analysis system. The individual core level fits include different chemical states and spin–orbit splitting for the constituent elements Cs, Te, and O by colour coding and in order of decreasing binding energy.

To calculate the chemical contribution of individual elements, we considered the main core level of each detected element in respect to their spectral areas, and then weighted them with relative sensitivity factors (RSF) in order to determine the atomic percentage represented by each element, as demonstrated by Yeh and Lindau [Yeh and Lindau, 1985]. We used the Casa XPS software package[4] to carry out this analysis.

From this data and the subsequent analysis, we conclude that the stoichiometry of the P1 Cs–Te cathode is approximately Cs_5Te_1. This implies that there is a significant excess of Cs on the surface compared to the ideal Cs_2Te stoichiometry. The XPS data suggests that this excess caesium is most likely to be present as a caesium oxide.

[4]Casa XPS v.2.3.22PR1.0 available from http://www.casaxps.com/

Table 1: Table showing the atomic composition of the P1 Cs–Te cathode measured using XPS in our surface analysis system after transfer from the TESS via a vacuum suitcase.

Element + State	State BE [eV]	Relative Contribution [%]	Atomic Composition [%]
Cs 3*d* $_{5/2}$	725.2	31.34	45.39
	725.9	19.4	
Cs 3*d* $_{3/2}$	739.1	27.11	
	740.5	14.46	
Te 3*d* $_{5/2}$	571.4 (Metal)	34.48	9.63
	572.9 (Sub–Oxide)	5.29	
	576.5 (Oxide)	14.9	
Te 3*d* $_{3/2}$	579.1	2.31	
	582.2 (Metal)	32.7	
	586.8 (Oxide)	10.31	
O 1*s*	531.7	100	23.95
C 1*s*	286.6	100	21.04

3.2 P3 Cs-K-Sb photocathode XPS

Figures 5 and 6 show the chemical composition and bond configuration for the P3 Cs-K-Sb photocathode. The major peaks for the elements detected are assigned, including the states originating from Cs, Sb, K, O and C. Comparatively, no traces of fluorine were detected which is contradictory to the XPS spectra taken at CERN on similar photocathodes [Panuganti et al., 2020]. This could be due to a number of reasons:

- the fluorine may have desorbed from the surface in the time between photocathode deposition and subsequent analysis at Daresbury;
- the instrument we used for this analysis may not have the sensitivity to resolve the fluorine signal;
- there may not have been any fluorine present during the synthesis of this particular photocathode.

In the analysis of the individual components, we have considered the spin–orbit splitting of p and d electrons. As can be seen, there is a significant level of surface oxidation, with oxygen accounting for 26.2 % of the surface signal compared to a level of 23.0 % measured at CERN. The data also shows that carbon contamination (C 1s = 287.0 eV) has increased dramatically from 7.3 % to 24.6 %. Weighting according to the respective RSFs,

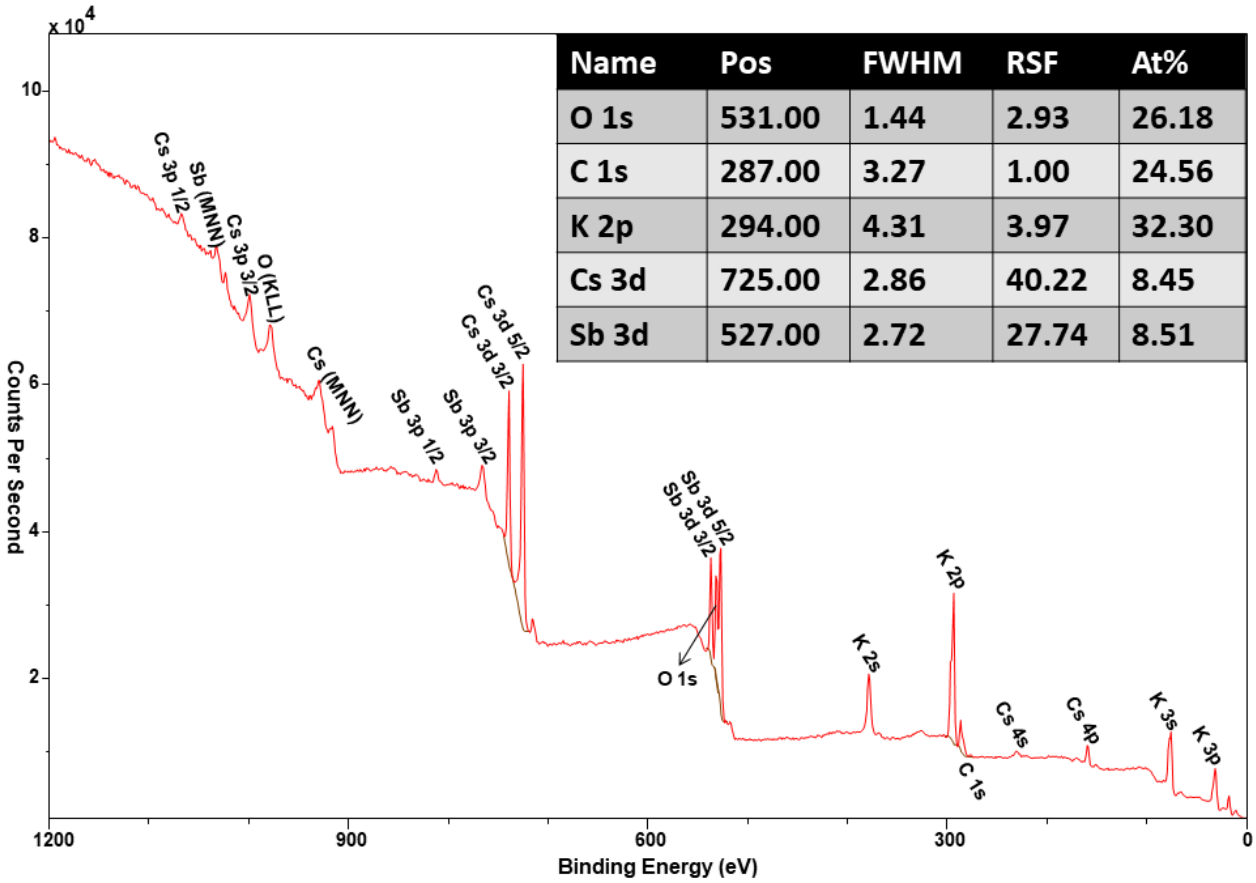

Name	Pos	FWHM	RSF	At%
O 1s	531.00	1.44	2.93	26.18
C 1s	287.00	3.27	1.00	24.56
K 2p	294.00	4.31	3.97	32.30
Cs 3d	725.00	2.86	40.22	8.45
Sb 3d	527.00	2.72	27.74	8.51

Figure 5: Full–range XPS survey spectrum with preliminary peak assignments for the P3 Cs–K–Sb photocathode.

we found the atomic percentage of Cs, Sb and K to be 8.5 %, 8.5 % and 32.3 % respectively. This demonstrates a marked decrease across all core elements, with the largest drop being a 9.8 % for Cs.

The reason for the shift in the C signal from 287.0 eV on the P3 Cs–K–Sb survey to 286.6 eV on the P1 Cs–Te survey is due to the nature of *adventitious carbon*. It has been documented well that the binding energies for particular bond structures such as C–O change between metals and exhibit a correlation with their work function where a lower work function shows a shift to larger binding energies[5].

The overall atomic composition for the P3 Cs–K–Sb cathode is shown in Table 2, and from this data we conclude that the stoichiometric ratio for the P3 Cs–K–Sb cathode is approximately $Cs_1K_4Sb_1$, though this excludes any oxides formed with the constituent elements of the photocathode, such as CsO. This data implies that there is an excess of alkali constituents as there are effectively 5 parts alkali metal group to 1 part pnictogen[6] group.

We expect that XPS analysis of the two remaining Cs–Te cathodes (P2 and P4) will be

[5]Shifting binding energies of adventitious carbon DOI: 10.1002/cphc.201700126

[6]A *pnictogen* is a member of the nitrogen group of elements (Group 15 of the periodic table), specifically nitrogen, phosphorus, arsenic, antimony, bismuth and ununpentium

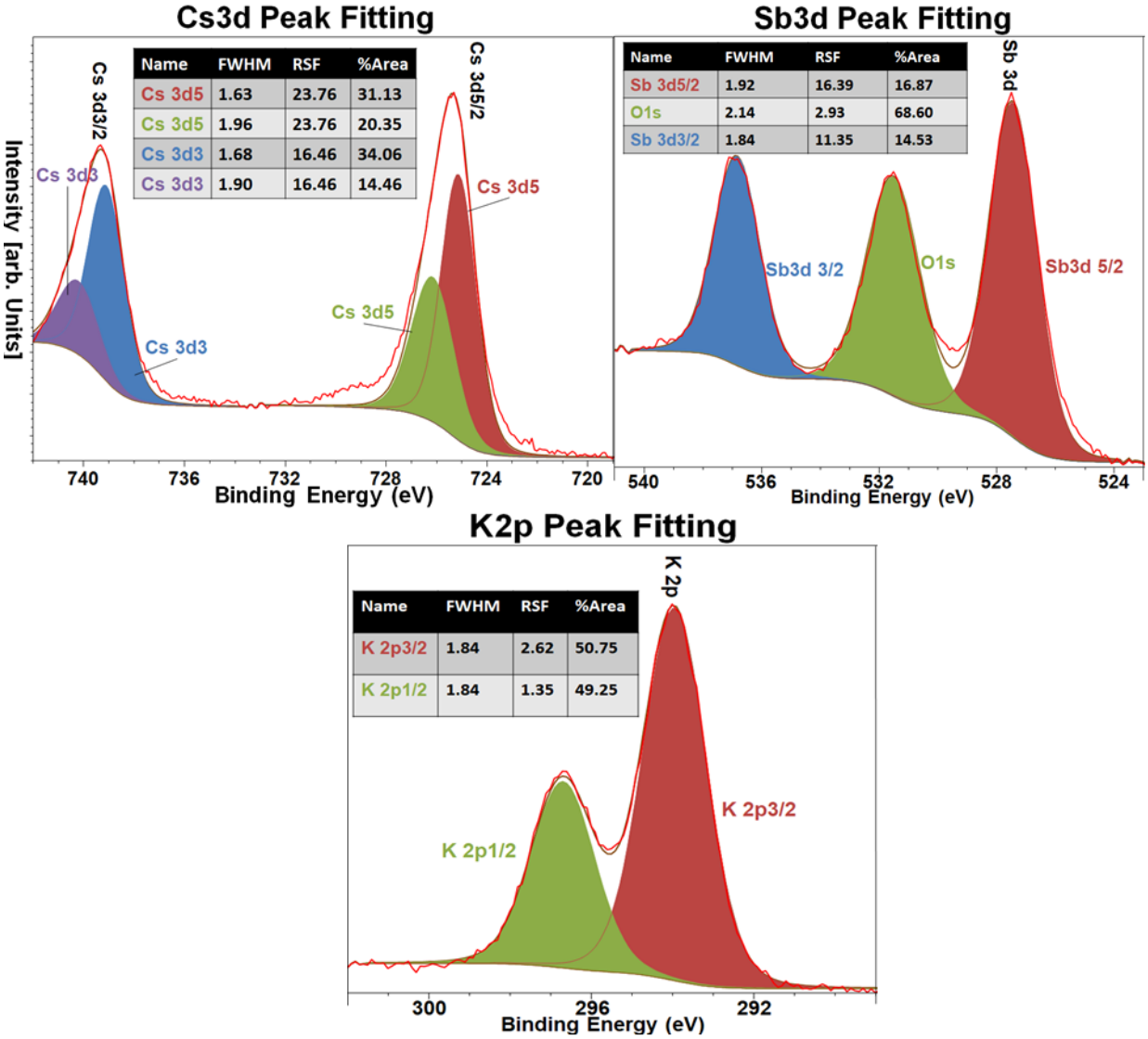

Figure 6: Peak fitting for the P3 Cs–K–Sb cathode. The XPS data was taken after transfer by vacuum suitcase from the TESS to our surface analysis system. The individual core level fits include different chemical states and spin–orbit splitting of the single elements Cs, O, Sb, and K by colour coding and in order of decreasing binding energy.

carried out as soon a practicably possible following the relaxation of the current (May ’20) Covid-19 restrictions.

Table 2: Table showing the atomic composition of the P3 Cs–K–Sb cathode following its transfer in a vacuum suitcase from the TESS to our surface analysis system.

Element + State	State BE [eV]	Relative Contribution [%]	Atomic Composition [%]
Cs $3d_{5/2}$	725.4	31.13	8.45
	726.5	20.35	
Cs $3d_{3/2}$	739.3	34.06	
	740.5	14.46	
Sb $3d_{5/2}$	527.7	100	8.51
K $2p_{3/2}$	293.2	100	32.30
O $1s$	531.5	100	26.18
C $1s$	287.0	100	24.56

4 STM Surface roughness measurements

This section contains an overview and analysis of surface roughness measurements taken using an Scienta Omicron UHV STM 1 in–vacuum STM for the P1 Cs–Te and P3 Cs–K–Sb photocathodes only. A complete summary of all STM line profile data taken during our analysis is presented for reference in Appendix B.

4.1 P1 Cs–Te photocathode STM

Figure 7 shows a series of images which summarise the topographical data taken for the P1 Cs–Te cathode in four different locations on the photocathode surface, where position 1 is at the photocathode centre and position 4 has the largest radial displacement from the centre. Each image was processed using the WSxM software[7] primarily to eliminate as much noise as possible through the use of a 'flatten' function which applies a correction to effectively smooth out minor noise in each image. The correction algorithm is proprietary, and one of three options can be applied during processing depending on the type of image being corrected. However this process is not able to eliminate any major artefacts in the scans. In addition to this, line profiles were taken for each individual scan to show local roughness on certain features of those scans taken.

Table 3 summarises the roughness analysis at each position measured with the corresponding roughness average (R_a) and RMS roughness (R_q) where:

$$R_a = \frac{\sum_{i,j} |a_{ij} - < a >|}{N} \qquad \text{and} \qquad R_q = \sqrt{\frac{\sum_{i,j} (a_{ij} - < a >)^2}{N}} \tag{1}$$

[7] WSxM software v.4.0 Beta 9.2 from http://www.wsxm.es/ used for this analysis

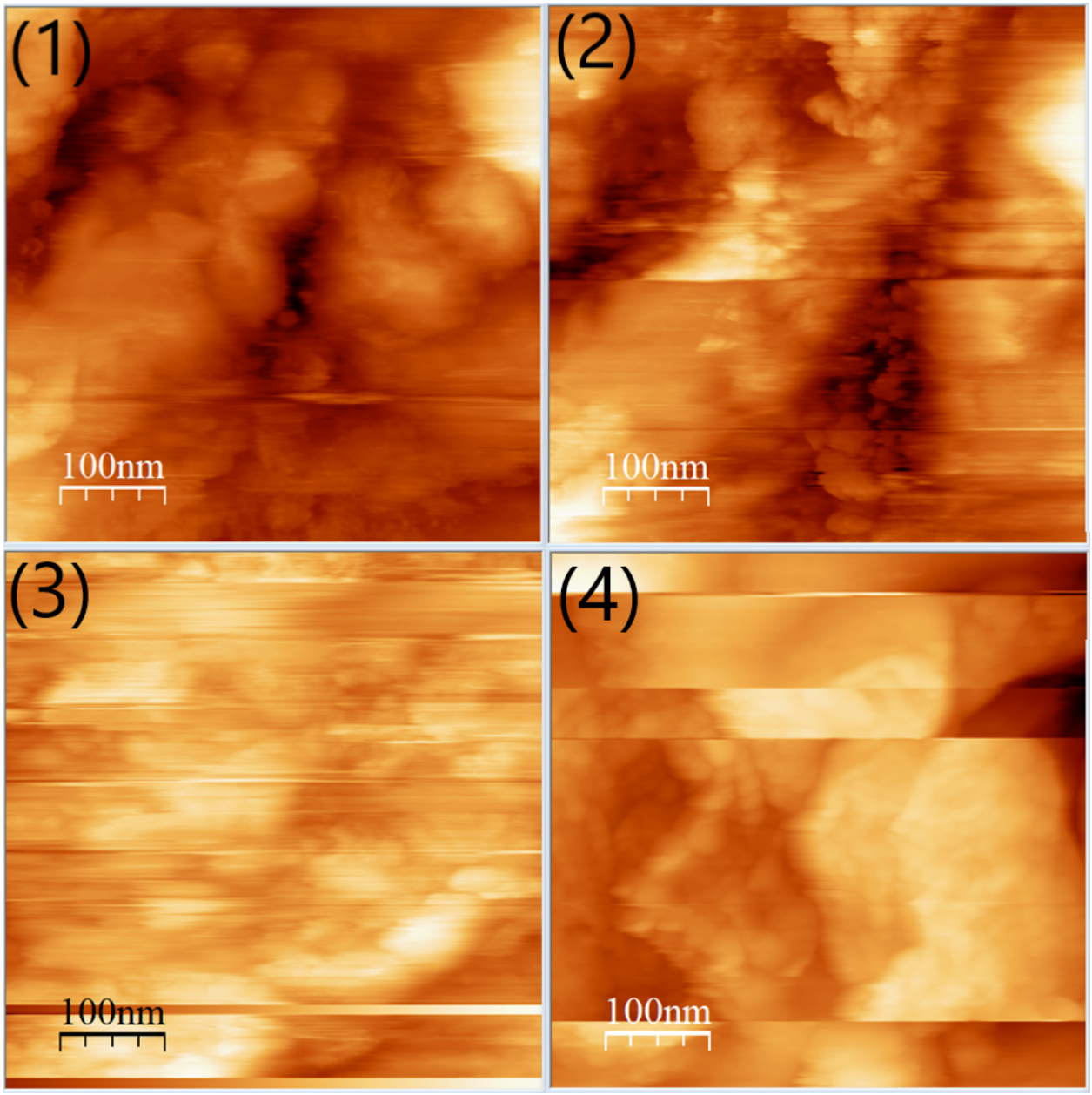

Figure 7: Surface roughness analysis using WSxM for the P1 Cs–Te photocathode at 4 different radial positions.

By definition, the roughness average is the mean of the absolute difference between the average height and the height of each single point of the sample scan. Consequently there is an element of noise which leads to varying levels of error in the scans, so only the cleanest scans obtained were used for this analysis. However there remain some notable errors in the images, and as such the corresponding line profiling of local regions in the scan as shown in Figure 8 are very important to show the roughness trend in the area characterised.

The reason that only the P1 Cs–Te photocathode was measured in the STM was due

Table 3: Table summarising the in–vacuum surface roughness measurements for the P1 Cs–Te photocathode.

STM Image	**Area [nm^2]**	**Roughness Analysis**	
		Average Roughness, R_a [nm]	RMS Roughness, R_q [nm]
Position 1	500	4.79	6.27
Position 2	500	4.75	5.93
Position 3	500	7.71	9.78
Position 4	500	13.56	16.61

to substrate mounting issues with the P2 and P4 Cs–Te samples. For these photocathodes, there was a significant level of protrusion and angular misalignment of the sample relative to its holder, such that it was not possible to accurately measure their surface roughness without causing damage to the STM probes as the required sample–tip compensation separation was beyond the range of the STM instrument.

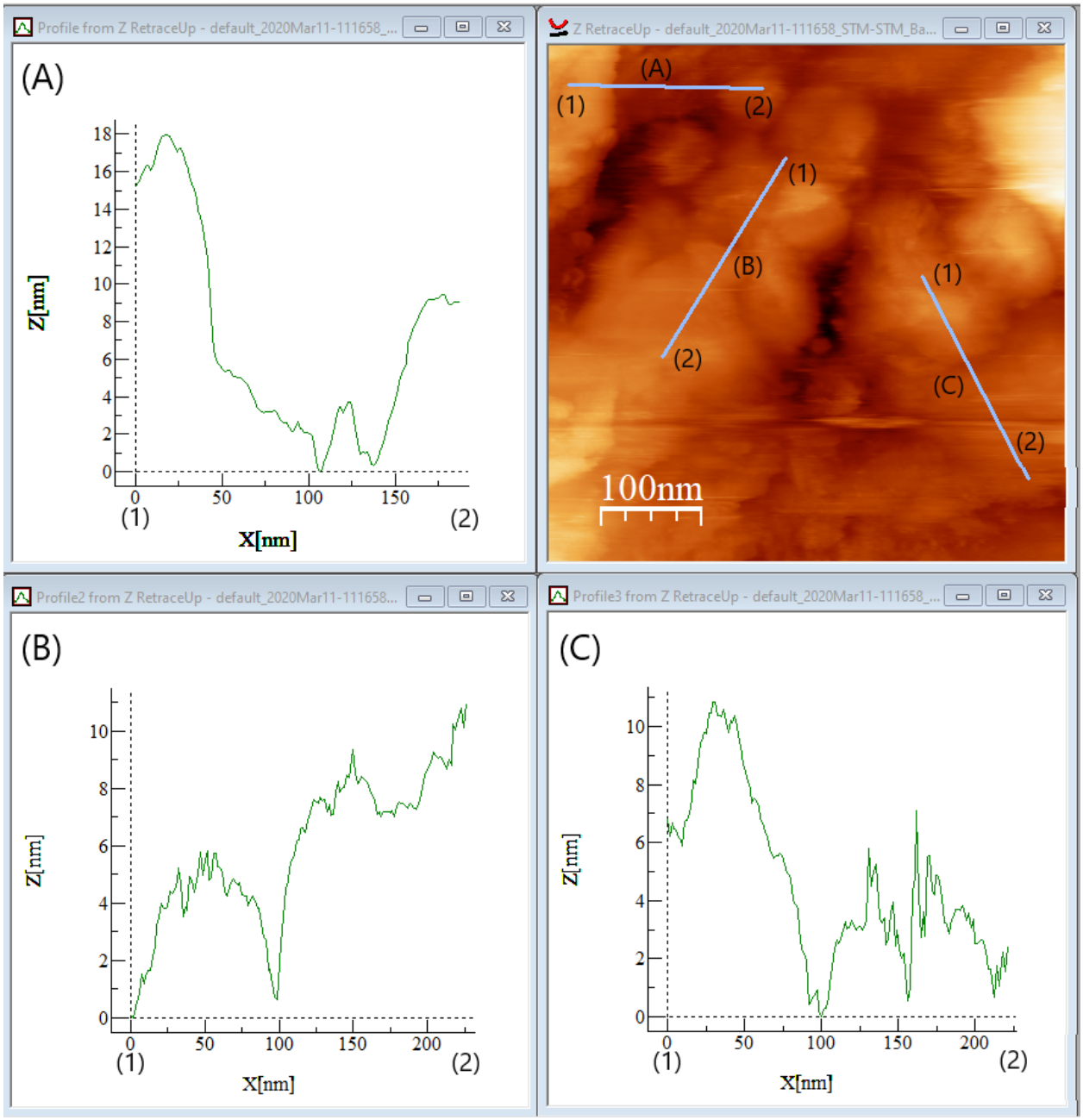

Figure 8: Surface roughness line profiles measured at position 1 on the P1 Cs–Te photocathode.

4.2 P3 Cs–K–Sb photocathode STM

Similarly to the P1 Cs–Te photocathode, the analysis for the P3 Cs–K–Sb cathode consists of scanning 4 positions from the centre (position 1) to as close to the edge as possible (position 4) as shown in Figure 9. Table 4 on page 16 shows the roughness values found for the P3 Cs–K–Sb photocathode.

Overall the P3 Cs–K–Sb photocathode exhibited a similar level of surface roughness to the P1 Cs–Te photocathode, however the line profiles generated for the P1 Cs–Te scans

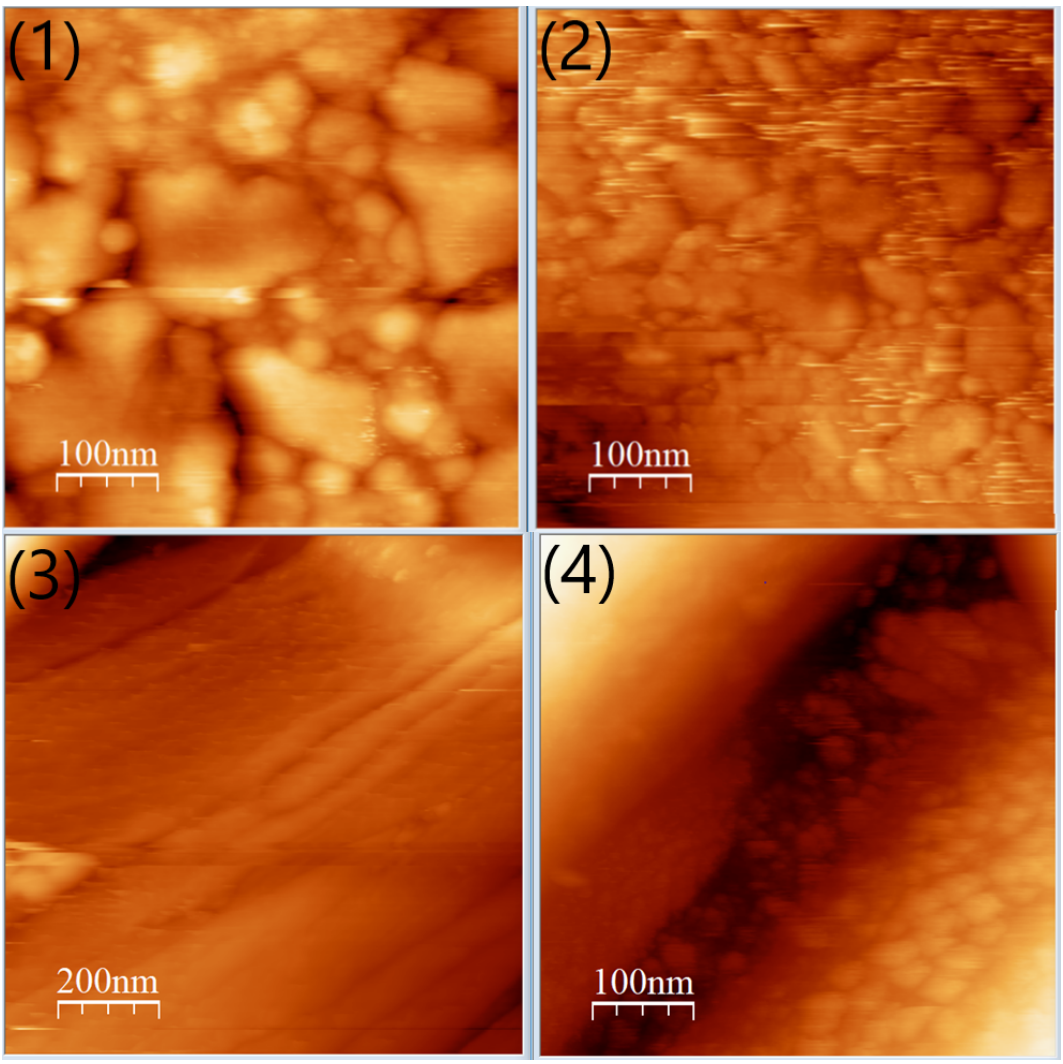

Figure 9: Surface roughness analysis using WSxM for the P3 Cs–K–Sb photocathode at 4 different radial positions.

generally showed higher levels of localised roughness than those for the Cs–K–Sb. This observation coupled with the increased noise level in the STM data suggests that the contamination on the P1 Cs–Te photocathode grows differently to that on the P3 Cs–K–Sb cathode, and is most likely related to the Te peak profile shown in Figure 4 where there may be varying levels of metal, oxide and sub–oxide sitting at the surface causing the artefacts seen in the P1 Cs–Te data.

The surface roughness of these two measured photocathodes followed the expected trend in that the average roughness increased as radial displacement from the cathode centre increased, with $R_a = 4.67\,\text{nm}$ near to the photocathode centre increasing to $R_a = 19.19\,\text{nm}$ closer to the edge for the P3 Cs–K–Sb photocathode, and the P1 Cs–Te photocathode showing similar results. This correlates with previous quantum efficiency measurements made at CERN where the QE was found to be highest at the centre and progressively fell towards the photocathode edge [Panuganti et al., 2020].

Table 4: Table summarising the in–vacuum surface roughness measurements for the P3 Cs-K-Sb photocathode.

STM Image	**Area [nm^2]**	**Roughness Analysis**	
		Average Roughness, R_a [nm]	RMS Roughness R_q [nm]
Position 1	500	4.67	5.91
Position 2	500	8.74	11.09
Position 3	1000	11.20	14.89
Position 4	500	19.19	23.11

This is further anecdotal evidence that the photocathode films are not uniform and the level of non–uniformity increases towards the extremities of the photocathode puck, though a measurement of surface roughness on a bare polycrystalline puck would be necessary in order to specifically exclude any contribution of substrate roughness to photocathode film roughness.

5 MTE Measurements

In order to obtain the mean transverse energy (MTE) from the photoemission footprint, the following procedure is carried out using the TESS system:

1. The photocathode under test is illuminated by a tuneable light source[8] over the range $\lambda = 200$ to 800 nm.
2. The light spot is focused to typically 0.1 mm diameter, and is considered to be a vanishingly small emission point for the purposes of the measurement.
3. The light beam delivered to the photocathode was adjusted using neutral density (ND) filters to avoid the effects of space–charge in the photoemitted electron beam and/or saturation in the MCP or the data acquisition camera.
4. Electrons are emitted from the cathode under test and drift between the source and the detector, covering a known distance (known as the *drift distance*).
5. The negative bias on the source and the positive bias on the detector are known, so with knowledge of the drift distance, the electron flight time can be calculated.
6. Electron emission is amplified using a microchannel plate whose output falls on a phosphor screen causing florescence. As such the detector is sensitive to a single photoelectron.
7. The image of the electron emission footprint is recorded using a data acquisition camera with a long exposure time, typically 60 to 120 s.
8. Analysis of the photoemission footprint coupled with the electron flight time is used to generate a transverse energy distribution curve (TEDC) to which a logarithmic curve is fitted.
9. The MTE is defined as the transverse energy at the $\frac{1}{e}$ point of the TEDC.

A extended description is presented in [Jones et al., 2017] and the commissioning of the experimental facility can be found in [Jones et al., 2013].

5.1 P1 Cs–Te photocathode MTE

Figure 10 shows the MTE values found as a function of the illumination wavelength for the P1 Cs–Te photocathode at room (red marks with grey fill) and cryogenic temperatures (blue marks with yellow fill). An OD 3.0 filter was placed in the light source for spectral measurements between $\lambda = 256$ and 406 nm wavelength at 297 K, with these points denoted by red squares. No ND filter was used for longer wavelengths with these points denoted by red circles. A corroboration measurement was taken with $\lambda = 406$ nm, one with an OD 3.0 filter inserted and one without, with these measurements yielding MTE values of 55.9 and 52.2 meV respectively.

[8] Energetiq EQ-99X laser–driven plasma broadband light source coupled using f–matched off–axis parabolic mirrors to a Bentham TMc300 monochromator

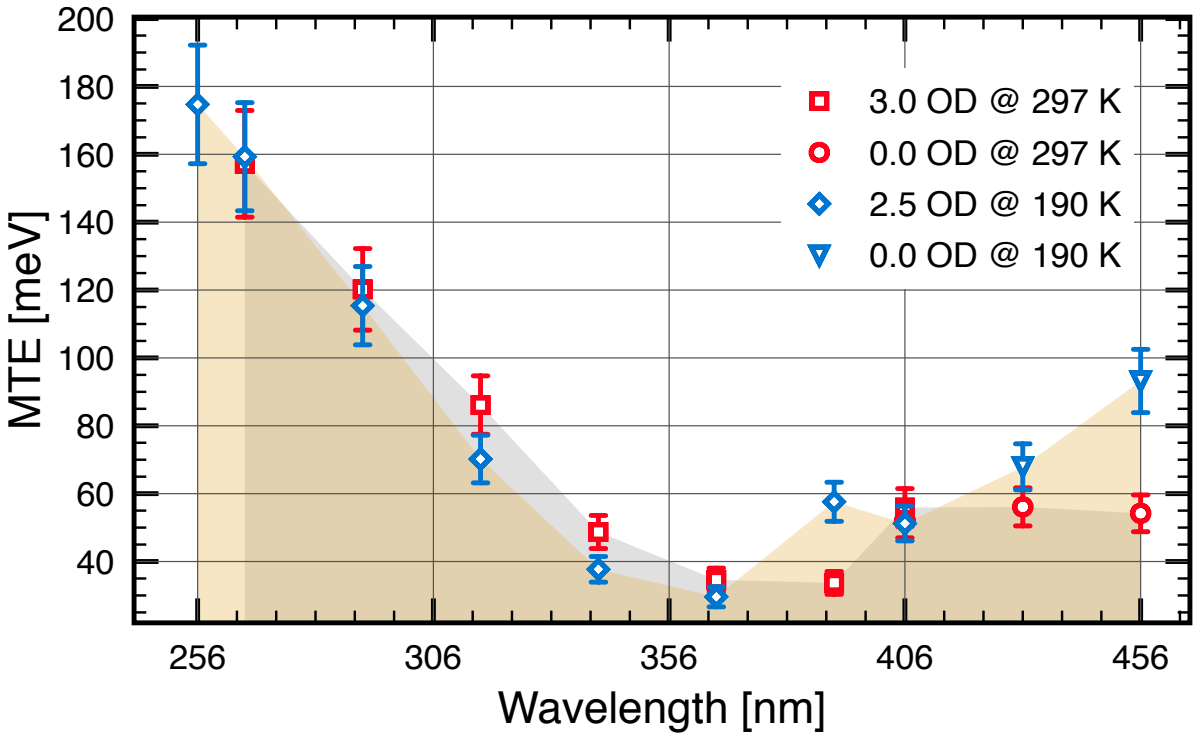

Figure 10: MTE values measured for the P1 Cs–Te photocathode.

The MTE was seen to progressively decrease as the illumination wavelength was increased over the spectral range $\lambda = 266$ to 391 nm, reaching its minimum value of 33.7 meV. The MTE was then seen to increase beyond 391 nm reaching a plateau just below 60 meV at longer wavelengths up to $\lambda = 456$ nm.

The MTE values measured at cryogenic temperatures (190 K) are shown in blue with yellow fill. An OD 2.5 filter was inserted in the light source for measurements over the spectral range $\lambda = 256$ to 406 nm, and these measurements are shown with blue diamonds. Two extra measurements were taken at $\lambda = 431$ and 456 nm which are represented by blue triangles. The MTE values obtained follow the same trend as those for room temperature measurements, progressively decreasing over the range 256 to 366 nm, with a minimum value of 29.6 meV at this longest wavelength.

For illumination wavelengths between 391 and 456 nm, the MTE values at cryogenic temperatures are higher than at the room temperature, except for the measurement at 406 nm which is lower. The MTE was again seen to increase in the last two measurements at the longest wavelengths, exceeding those taken at room temperature. The MTEs measured for this cathode largely exhibit a thermal independence such that in broad terms, the same values are recorded irrespective of photocathode temperature. This trend breaks down at longer illumination wavelengths which are outside of the accepted spectral response wavelength range for a Cs–Te photocathode. We believe that the formation of low work function CsO_2 surface layer (a highly polar molecule with a strong intrinsic elec-

tric dipole) may drive this behaviour at long wavelengths, and the XPS data presented in section 3.1 appears to support this premise.

Based on the change in filter optical density used during these measurements, we believe that the QE was 1000 times higher at the shorter wavelengths (red squares) than that at longer ones (red circles), falling to a factor of approximately 300 (based on the use of an optical density of 2.5) for the cryogenic measurements. This basic inference assumes a constant light source intensity is delivered over these wavelengths at both room and cryogenic temperatures, though realistically based on data from the equipment manufacturer, there is approximately a factor of two difference in the light source intensity in this spectral region.

The MCP gain is controlled by the difference between the voltages applied to the front and back plate of the device, with gain approximate doubling with every 50 V increase in the difference between the front and back plates. The MCP back voltage was adjusted to compensate for the differing filter optical densities used during these measurements to maintain a similar level of intensity at the data acquisition camera for each wavelength measured. We attribute the apparent fall in QE which was compensated by increased MCP gain as being due to the detrimental affects of cryopumping contaminating the cooled photocathode surface.

5.2 P2 Cs–Te photocathode MTE

Figure 11 shows the MTE values measured at room and cryogenic temperatures for the P2 Cs–Te cathode. The first set taken at 297 K (red squares on grey fill) and the second set at 213 K (blue triangles on purple fill). Both data sets were acquired with an OD 2.0 filter placed in the light source and compensation applied to the MCP back voltage in order to maintain a similar intensity level in the detector camera at each wavelength. A decrease in MTE was observed for shorter wavelengths, reaching a minimum at $\lambda = 431$ nm with 67.8 meV. Photoemission was again seen at longer wavelengths which should strictly be outside of the accepted spectral response for a Cs_2Te photocathode, with the MTE increasing to 85.3 meV at 532 nm.

Measurements at 213 K with cryogen flowing are shown in blue triangles with purple fill. They follow the same trend at shorter wavelengths as those measurements made at room temperature, reaching a minimum MTE of 96 meV at $\lambda = 341$ nm. The MTE is then seen to rise to a local maximum of 134 meV around 431 nm which is where the minimum MTE was found in the room temperature measurements. A final measurement with $\lambda = 532$ nm yielded an MTE of 104 meV which is in rough agreement with the room temperature measurement when the limits of the respective error bars are considered.

A further room temperature measurement was made using a 532 nm laser which yielded an MTE of 83.4 meV, giving excellent agreement with the previous measurement of 85.3 meV at this wavelength using the broadband lightsource and monochromator to illuminate the photocathode. A similar measurement using the laser to illuminate the cathode under cryogenic conditions was not made.

It is not clear why we saw clear photoemission at this wavelength as $\lambda = 532$ nm lies some way outside the spectral response curve for a Cs_2Te photocathode [Gaowei et al., 2019]. In contrast to the P1 cathode, this cathode presents thermally–dependent beha-

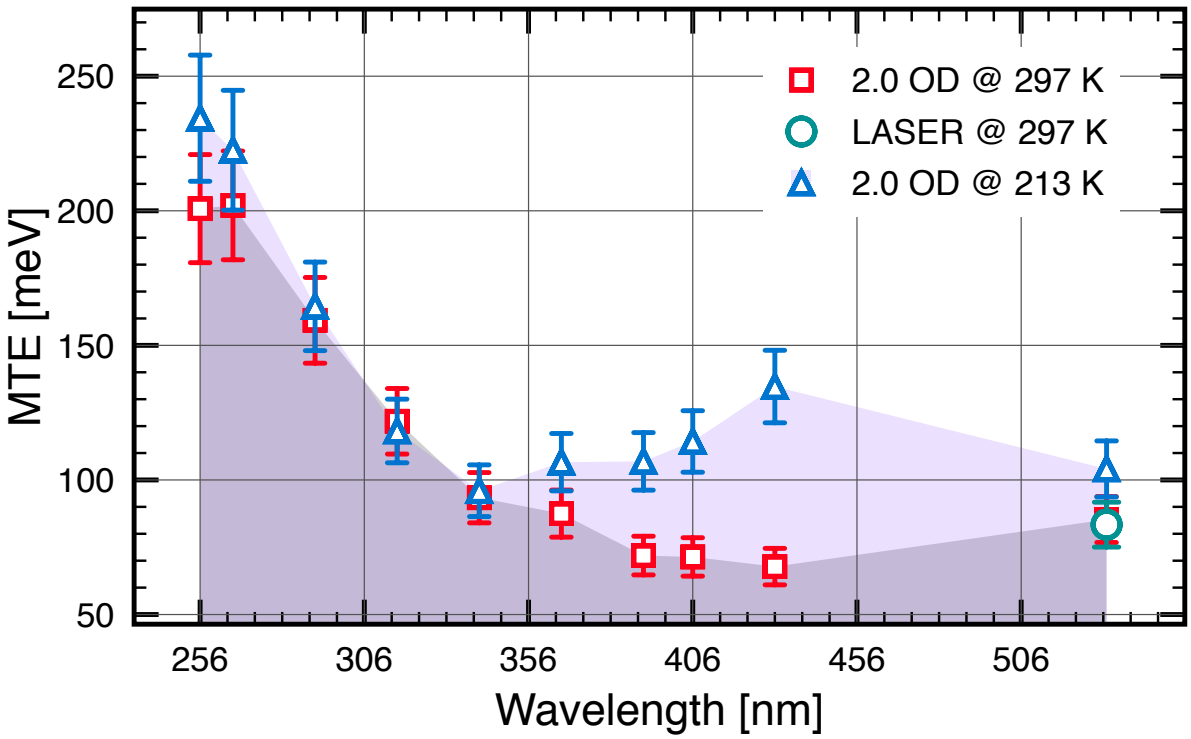

Figure 11: MTE values measured for the P2 Cs–Te photocathode.

viour characteristics over a substantial wavelength range. Once again, it is possible that a formation of a highly–polar low work function CsO_2 surface layer might have occurred. Further XPS measurements once the Covid-19 restrictions are relaxed may provide more evidence, though the surface will obviously have degraded significantly during the Covid lock–down.

5.3 P4 Cs–Te photocathode MTE

Figure 12 shows the MTE values found for measurements at 297 K in red and at 208 K in blue. An OD 2.5 filter was used in the room temperature measurements for $\lambda = 256$ to 366 nm and for $\lambda = 256$ to 406 nm under cryogenic conditions. No filter was used for measurements at the longer wavelengths and these are shown using red circles and blue triangles for the room and cryogenic measurements respectively in the presented data. A corroboration measurement was made at 366 nm with and without an ND filter which yielded MTE values of 76.2 meV and 79.3 meV respectively, giving good agreement with data taken during the main data acquisition runs. The change in the filter optical density required for correct operation of the TESS instrument without space charge implies that the QE was around 300 times higher at the shorter UV wavelengths than that at the longer visible wavelengths.

The data show a progressive decrease in MTE with a minimum of 75.7 meV at $\lambda =$

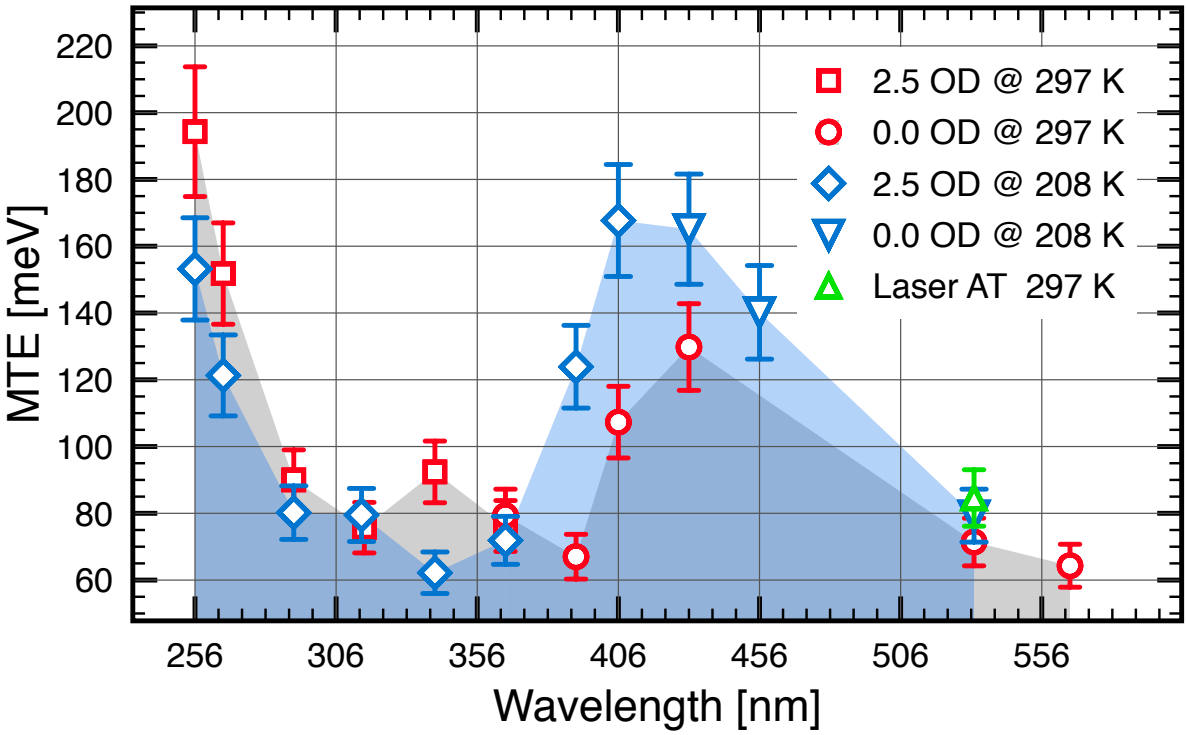

Figure 12: MTE values measured for the P4 Cs–Te photocathode.

316 nm. A subsequent maximum of 92.4 meV is found at 431 nm for the room temperature measurement, with a higher and perhaps unexpected maximum of 129.8 meV for the cryogenic measurement at this wavelength. Following this the MTE fell progressively, reaching a minimum value of 64.3 meV at $\lambda = 556$ nm, this being the longest wavelength measured.

During cryogenic measurements made with the photocathode at 208 K, an OD 2.5 filter was again placed in the optical path over the wavelength range $\lambda = 256$ to 406 nm. This data is represented by the blue diamonds with blue fill in Figure 12. The filter was removed for measurements at longer wavelengths which are denoted by blue triangles with blue fill. The trend in the MTE values measured when the photocathode was cooled follows that seen in the room temperature measurements, albeit with the measured MTE being slightly lower over the UV range range $\lambda = 256$ to 366 nm. The minimum MTE was found to be 62.2 meV at 341 nm. The MTE values measured over the visible range with $\lambda = 391$ to 532 nm are higher than those measured at room temperature over the same wavelength range. As such, this photocathode exhibits an unexpectedly high degree of thermal dependence in its MTE, and while the reasons for this are unknown at present, some insights may be possible if XPS analysis is carried out for this photocathode to determine the surface stoichiometry.

A single measurement at room temperature using a 532 nm laser was performed for comparison to the previous room and cryogenic temperature measurements at this wavelength

which both used the broadband light source and monochromator to illuminate the photocathode. The laser has significantly more optical power and so required additional ND filters to attenuate the beam and avoid detrimental effects of space charge, and also has a smaller spectral linewidth (c. 0.1 nm for the laser compared at ~ 1.4 nm FWHM for the broadband source and monochromator). The MTEs found were 71.4 meV, 84.6 meV and 79.3 meV respectively, demonstrating a good level of agreement and validating our initial measurement.

The MTE values measured at 266 nm should be taken as the reference values for the Cs–Te photocathode class as this is the typical illumination wavelength used in a working photoinjector electron gun, set by the constraints of current laser technology. Based on our results, we report the reference MTE values as being 152 meV at 297 K and 121 meV at 208 K.

5.4 MTE Summary for the Cs–Te photocathodes

Figure 13 summaries the MTEs measured as a function of illumination wavelength for the P1, P2 and P4 Cs–Te photocathodes at both room temperature (top) and while cryogenically cooled using nitrogen vapour (bottom).

The upper plot shows that the trend in MTE measured for all three photocathodes follow broadly the same pattern when illuminated at the short UV wavelengths, but beyond $\lambda = 391$ nm the photocathodes present differing responses. Photocathode P1 exhibits its lowest MTE of 34 meV at 391 nm, and samples P1 and P4 exhibit similar behaviour with MTEs for both increasing at wavelengths longer than 391 nm. Beyond this wavelength, the MTE for the P1 photocathode plateaus to around 55 meV while that for the P4 cathode rises sharply to a maximum of 130 meV around 431 nm before falling again and reaching a minimum around 65 meV at 566 nm. The P4 photocathode exhibits a substantial increase in MTE at these longer wavelengths, and also shows a degree of temperature dependence as the MTE is even higher when the sample is cooled.

In order to exclude the possibility that the monochromator was passing second order light at the longer visible wavelengths, the broadband light source was substituted for a 532 nm laser and MTE measurements repeated for the P1 and P4 cathodes. This ensured that the photocathodes only received illumination from long–wavelength visible light at 532 nm (with no possibility of a UV second harmonic), and both MTEs measured in this experiment were found to be in the region of 34 meV. However this behaviour was not expected as photoemission should not occur at these longer (visible) wavelengths, suggesting that the composition of the photoemissive layer is not limited to Cs_2Te.

When subjected to cryogenic cooling, the three photocathodes again exhibit broadly similar behaviour under illumination at short UV wavelengths with their MTEs progressively falling until a minimum is reached in the 346 nm to 356 nm region. At wavelengths longer than this, their MTEs rise though the behaviour of each cathode is unique to some extent. Photocathode P4 exhibits the lowest MTE of all the cathodes tested at the shortest UV wavelengths, but the fact that it exhibits strong photoemission with high MTE at longer visible wavelengths implies that there is a significant excess of Cs on the pho-

tocathode surface (much more than is strictly required for a Cs_2Te surface) or other low work function Cs–Te compounds, and it is these which are primarily responsible for photoemission with high MTE at visible wavelengths.

None of the cathodes were re–tested using the 532 nm laser while cooled as it was felt that this point had already been investigated with the cathodes at room temperature.

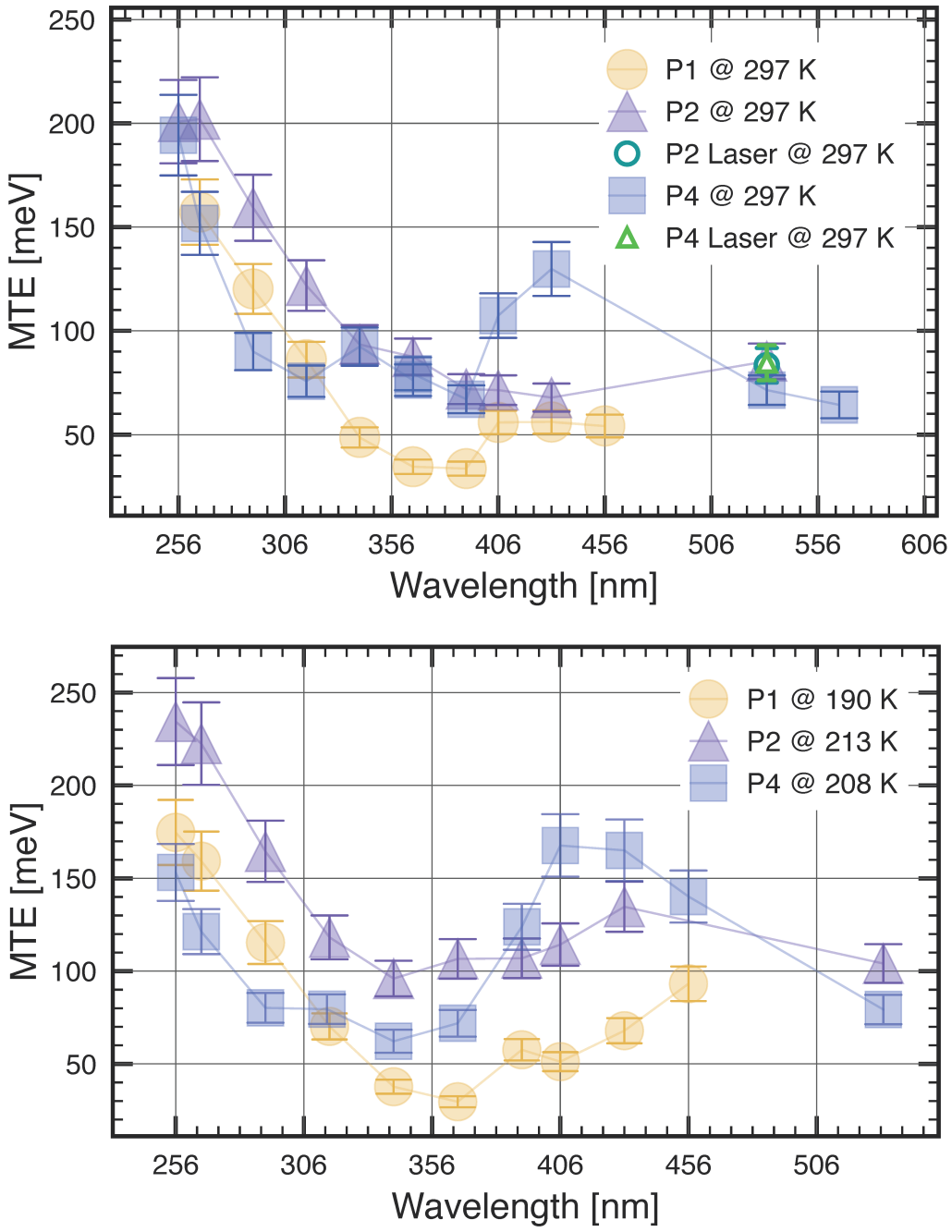

Figure 13: Summary of MTEs measured for the P1, P2 & P4 Cs–Te photocathodes.
Top: Photocathode MTE values measured at room temperature (297 K).
Bottom: Photocathode MTE measurements when cooled with nitrogen vapour (c. 200 K).

5.5 P3 Cs–K–Sb photocathode MTE

5.5.1 Cs–K–Sb photocathode QE

Prior to performing TEDC measurements for the P3 Cs–K–Sb cathode, the QE was measured at 532 nm in our III-V semiconductor PPF. This suggested an initial value around 0.0024 % which is extremely low for a photocathode of this class. The sample was then transferred into the TESS and TEDC measurements were performed, with results as described in section 5.5.2. The photocathode was then moved back to the PPF for a further QE measurement, during which the cathode also exposed to gentle controlled heating to around 100 °C while monitoring the QE.

Figure 14 summarised the outcome of our QE measurements at 532 nm. All of the QE measurements were made over a small area with a laser spot diameter of slightly less than 1 mm. The data clearly show that the QE increased under moderate and controlled heating, rising from 0.0024 % at room temperature to 0.0056 % at around 100 °C over a 20 minute period. The laser was switched off briefly during the heating phase to confirm that the response seen was genuine photoemission from the cathode.

For times beyond T = 1,400 seconds, the laser position on the photocathode was moved and it was noted that there was a high level of variability in the QE indicating non–uniformity across the photocathode surface.

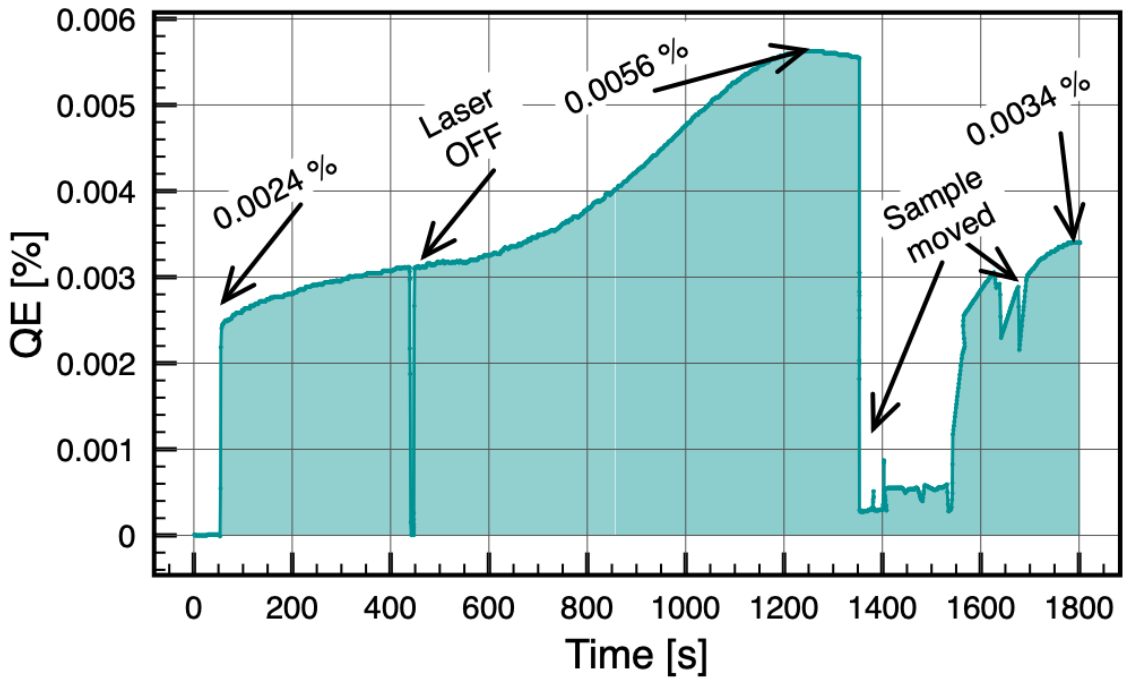

Figure 14: Summary of QE measurement results for the P3 Cs–K–Sb photocathode under illumination at 532 nm wavelength.

5.5.2 Cs–K–Sb photocathode MTE

It was expected that the relatively high QE for a cathode of this class combined with the high level of optical power available from the broadband light source and monochromator in the visible region, a high level of attenuation to the light source would be required to avoid space charge affecting the MTE measurements. This was achieved in part by using a neutral density filter (as previously for measurements on the Cs–Te cathodes at UV wavelengths), but also by reducing the size of the monochromator output aperture which has the consequence of both reducing the output intensity and decreasing the spectral bandwidth of the light source. A filter with OD 1.2 was used for these measurements.

MTE was only measured for this cathode at room temperature. The bi–alkali class of cathode is more susceptible to contaminant poisoning than the Cs–Te class, and the act of cooling was expected to dramatically increase surface contamination through cryo–pumping. The QE on arrival at DL after transportation in the vacuum suitcase was found to be in the region of 0.002 % which is already very low, and we took this decision to avoid reducing the QE any further.

Figure 15 shows the MTE values measured over a broad range of illumination wavelengths from $\lambda = 442$ nm to 682 nm in 10 nm steps. The MTE can be seen to decrease progressively to a minimum value of 55 meV at 572 nm, with an un–expected step to a local maximum at 582 nm, followed by a reduction to a value close to the minimum before the MTE then

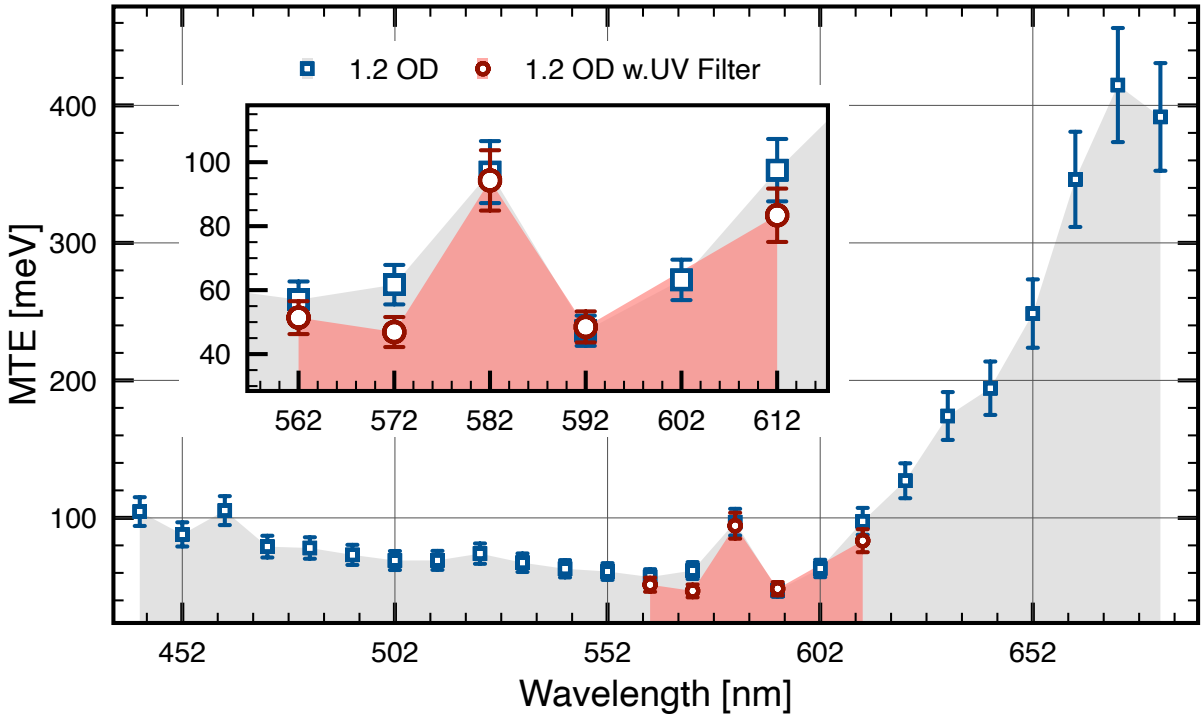

Figure 15: MTE values measured for the P3 Cs–K–Sb photocathode.

progressively increases to very large values as the illumination wavelength is increased further.

To investigate the step at 582 nm, a UV filter was inserted in the light source to ensure that any short wavelength or second–order output from the monochromator was blocked. As can be seen from the inset in Figure 15 which shows these second measurements as red circles, very similar MTE values were obtained. This indicates that the illumination light source is spectrally–pure so the MTE is not driven by a low intensity short wavelength UV component passing through the monochromator. The step at 582 nm remains un–explained.

6 Caesiation of a polycrystalline copper sample

In order to better understand the MTE values presented in the previous section, and to gain an insight into the photoemissive response of a caesium overlayer on a copper substrate identical to that used for the Cs–Te and Cs–K–Sb photocathode growth at CERN, we carried out a study using the Cs dispensers in our III-V semiconductor photocathode preparation facility (PPF)[9] on a spare copper puck from the same batch as those supplied to CERN, and then examined the photoemission characteristics using the TESS.

The polycrystalline photocathode sample puck (referred to as Cu Poly) was prepared in the Multiprobe system. The puck was first argon–ion bombarded to remove contaminants (Ar^+ for 20 minutes with 2.0 μA drain current), then annealed at around 650 °C for 1 hour, and its surface examined using XPS to ensure cleanliness. This cycle was repeated until a clean XPS survey scan was obtained. The puck was then transferred into the GaAs PPF under UHV conditions via a vacuum suitcase maintaining a pressure in the low 10^{-10} mbar region. It was then heat–cleaned following the same temperature profile as that used previously for annealing in the Multiprobe system, and once cool, it was was transferred into the TESS for energy distribution measurements. The measurements were carried out in three stages with the sample transferred back from the TESS into the PPF between each stage for Cs deposition as described previously [Jones et al., 2017]. The stages of the experiment were:

1. Clean Cu Poly puck MTE measured at $\lambda = 266$ nm;
2. Caesium applied to the Cu Poly puck for 7 minutes with the Cs sources operated at a current of 2.8 A. The puck was then moved into the TESS for MTE measurements at $\lambda = 266$ nm and 532 nm;
3. Caesium applied for a further 40 minutes, and the puck then moved back into the TESS for MTE measurements at $\lambda = 266$ nm and 532 nm.

Figure 16 shows the visual appearance of the Cu Poly puck after each of the three stages described. The photographs were taken with the puck in the PPF activation chamber immediately prior to its transfer into the TESS for MTE measurements. The lighting conditions, camera position and exposure were ostensibly the same for all of the photographs. There is a noticeable change of colour and reduction in surface reflectivity in the second and third photos due to caesium deposition.

Figure 17 shows the five transverse energy distribution curves (TEDC) measured for the Cu Poly photocathode. It should be noted that these are the actual TEDC extracted from the TESS measurements, and not curves fitted to the TEDC. Consequently the TEDC shown contain structure due to the presence of the grid mounted on the front of the TESS detector.

The integrated area under each curve (A) is shown for all curves to facilitate quantitative comparison of the photoemissivity of the surface. The black curve corresponds to the first stage where the sample was clean (prior to Cs deposition), and exhibits a fairly

[9] Two SAES alkali metal dispensers connected in series, mounted side–by–side

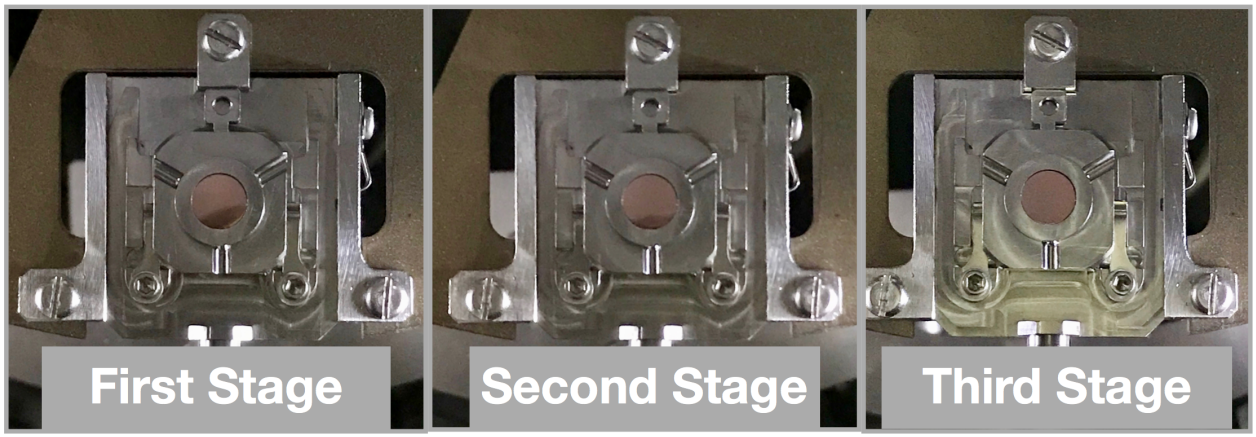

Figure 16: Photographs of the Cu Poly photocathode puck:
First Stage shows the clean surface prior to the initial measurement;
Second Stage shows the puck after Cs deposition for 7 minutes;
Third Stage shows the puck after a 40 minutes of Cs deposition.

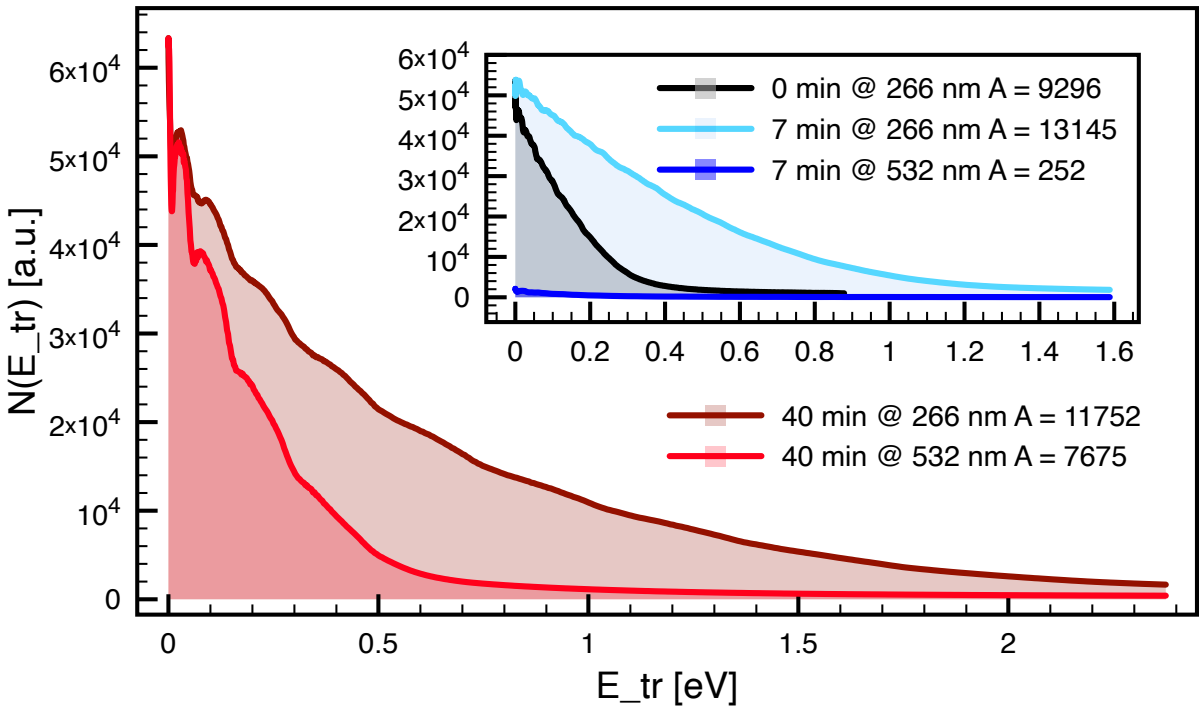

Figure 17: Transverse energy distribution profiles for the Cu Poly photocathode puck following staged exposure to caesium. The 'A' value corresponds to the integrated intensity under the respective curve, allowing quantitative analysis of the effects of Cs deposition.

typical TEDC for clean copper under illumination at 266 nm. The blue curves correspond to the second stage, with the lighter blue showing the response at 266 nm and the darker blue at 532 nm. It is noticeable that the level of photoemission is low for the visible wavelength, and in order to facilitate this measurement the MCP back voltage was increased in comparison to that used for the measurements at UV wavelengths. The red curves correspond to the third stage, with the dark red showing the response at 266 nm and the bright red at 532 nm. It is clear that the deposition of caesium onto the Cu Poly puck has dramatically increased the level of photoemission from this sample under illumination at 532 nm.

A comparison of the integrated intensities after the 40 minute Cs exposure shows a difference between the total photoemission at 532 nm to that at 266 nm of around 0.65, compared to just 0.02 for the 7 minute Cs exposure. This result shows that Cs on Cu photoemits readily, and if sufficient Cs is present on the surface then the total level of photoemission at 532 nm is a significant fraction of that seen at 266 nm. We therefore conclude that following deposition of Cs and Te to create a Cs–Te photocathode, any excess Cs will readily emit electrons when illuminated by visible light.

Table 5 summaries the MTE values extracted from each of the TEDC shown in Figure 17. The data clearly show that the MTE of electrons photoemitted from caesium are extremely high due to its very low work function, and the overall MTE increases further with coverage. The PPF chamber where caesiation took place and the TESS experimental chamber are both maintained in the XHV pressure region, but the increase in MTE due to caesium coverage might be linked to the formation of Cs–O surface dipoles over time as several hours elapsed between the second stage and third stages of the experiment. The doubling of photon energy when illuminating this cathode at UV wavelengths drives a massive increase in MTE due to the significant excess energy in photoemission from the deposited caesium. It is likely that this also occurs in the CERN photocathodes with the excess caesium contributing a relatively small number of electrons to the photoemission footprint, but with these electrons having a significant level of MTE under illumination at UV wavelengths.

The concept of excess energy is explored further in Appendix A, though no final conclusions are drawn on this.

Table 5: Summary of the MTE values measured for the Cu Poly sample.

Wavelength, λ [nm]	**Cu Poly**, MTE **[meV]**		
	First Stage	**Second Stage**	**Third Stage**
266	166	497	584
532	-	164	225

7 Summary of results

In this section we present a summary of the measurements made on the four photocathodes characterised in this study. This takes the form of a series of tables containing the relevant values corrected to 3 significant figures to ease comparisons.

Table 6: Atomic composition of the P1 Cs–Te photocathode from XPS data.

Element and State	**Atomic Composition [%]**
Cs 3*d*	45.4
Te 3*d*	9.63
O 1*s*	24.0
C 1*s*	21.0

Table 7: Surface roughness of the P1 Cs–Te photocathode from STM data.

		Roughness Analysis	
STM Image	**Area [nm^2]**	Average Roughness, R_a [nm]	RMS Roughness, R_q [nm]
Position 1	500	4.79	6.27
Position 2	500	4.75	5.93
Position 3	500	7.71	9.78
Position 4	500	13.6	16.6

Table 8: MTE values measured for the Cs–Te photocathodes.

Illumination Wavelength, λ [nm]	**MTE [meV] at Temperature [K]**					
	Cathode P1		**Cathode P2**		**Cathode P4**	
	297 K	190 K	297 K	213 K	297 K	208 K
266	157	159	202	223	152	121
406	56	93	71	114	107	168
532	-	-	85	104	71	79

Table 9: Atomic composition of the P3 Cs–K–Sb photocathode from XPS data.

Element and State	**Atomic Composition [%]**
Cs 3*d*	8.45
Sb 3*d*	8.51
K 2*p*	32.3
O 1*s*	26.2
C 1*s*	24.6

Table 10: Surface roughness of the P3 Cs–K–Sb cathode from STM data.

STM Image	**Area [nm2]**	**Roughness Analysis**	
		Average Roughness [nm]	RMS Roughness [nm]
Position 1	500	4.67	5.91
Position 2	500	8.74	11.1
Position 3	1000	11.2	14.9
Position 4	500	19.2	23.1

Table 11: MTE values measured for the P3 Cs–K–Sb cathode.

Illumination Wavelength, λ [nm]	**MTE [meV]**
442	105
532	67
682	392

8 Conclusions

The Cs–Te photocathode samples received at Daresbury exhibit a high degree of variability, evidenced by the visual differences in the optical properties of the photoemissive layer as shown by the photographs in Figure 2, and by the surface characterisation and electron emission performance measurements made in this study. At the time of their manufacture (Spring 2020), the CLIC/CTF3 photocathode deposition system at CERN was undergoing a software and controls upgrade which had only been partially completed. It is likely that this is the primary reason for the variability seen in these photocathodes, and also for some of the differences in the Cs–K–Sb source grown for this study when compared with other bi–alkali photocathodes grown by CERN.

8.1 Cs–Te photocathodes

Our MTE measurements on the Cs–Te photocathodes show a good level of consistency at both room and cryogenic temperatures when under illumination at UV wavelengths. However, we found that these Cs–Te photocathodes readily emit at longer wavelengths beyond 400 nm, and that the MTEs measured over this spectral range are large. Furthermore the differences found between the MTE for each of the Cs–Te photocathodes are dramatic at the longer wavelengths, as are the performance differences measured for some cathodes at room and cryogenic temperatures.

The fact that there is clear and relatively strong photoemission at visible wavelengths which should be outside of the spectral response range for a Cs_2Te photocathode with correct stoichiometry implies that there is an excess of caesium and/or Cs_xTe_y compounds present in the photocathode surfaces. Based on the evidence for photoemission from caesium explored in Section 6 and our XPS data for the P1 cathode, we suggest that the excess caesium is photoemitting electrons which exhibit high levels of MTE due to the caesium's low work function, particularly when illuminated at UV wavelengths where the excess energy is large. This is explored in greater detail in appendix A. Photoemission at the visible wavelengths is also attributed to the caesium excess, but with a lower of .

We suggest that the notable differences in MTE for the Cs–Te photocathodes at cryogenic temperatures may be due to the formation of Cs–O molecules on the cathode surface. Caesium is known to be reactive with a strong affinity for oxygen, and the formation of Cs–O compounds will be accelerated through the mechanism of cryo–pumping when the photocathode is cooled. If the excess caesium were to form highly–polar Cs–O molecules with an effective workfunction even less than that for Cs (2.14 eV, Michaelson, 1977), these will drive an increase in both QE and MTE over the visible spectral range. Our MTE measurements appear to agree well with the Cornell approximation (see equation 2 in Appendix 'A') if the assumed workfunction of the photoemission source is similar to or slightly less than that of Cs.

Of course a Cs–O surface layer may have formed during the transportation of the cathodes to Daresbury as the ambient pressure (and therefore the partial pressure of oxygen) in the transport system is likely to be higher than those pressures in the PPF and TESS vacuum systems which are in the mid 10^{-11} and 10^{-12} mbar regime respectively. However this in itself does not explain why the MTE response for the P2 and P4 cathodes differ so

obviously at cryogenic temperatures compared to room temperature without considering the possible effects of cryo–pumping during the 'cold' measurements which were made *after* those at room temperature.

Cathode P1 exhibited the lowest level of thermal dependence in its response, with its room and cryogenic MTE values being quite similar despite the XPS data indicating that there was a significant level of excess caesium present. In contrast, cathodes P2 and P4 exhibited a high level of thermal dependence in their MTE. Based on this premise, we believe that cathode P4 had the largest caesium excess due to the clear thermal dependence in its MTE and the magnitude of the MTE values found. We hope that this can be further investigated and evaluated using XPS in the near future following the lifting of Covid-19 working restrictions.

We were unable to carry out QE measurements at $\lambda = 266\,\text{nm}$ using our UV laser system due to some issues with the laser system setup. However, based on the experimental parameters during MTE measurements (specifically the reduction in filter optical density, but also the detector gain), cathode P2 appeared to have the lowest QE of the Cs–Te photocathode samples, though we are unable to place a specific value on this.

8.2 Cs–K–Sb photocathodes

The P3 Cs–K–Sb bi–alkali photocathode exhibited a very low level of MTE when illuminated at wavelengths up to around 570 nm. It is likely that the QE was extremely low which will have served to reduce the MTE of emitted electrons, but this cathode also exhibited very high levels of MTE under illumination at wavelengths beyond 580 nm.

While no direct QE measurement for this cathode was made following growth at CERN, previous work has delivered QEs in the region of 6 % at 532 nm, and it was felt at the time of growth that the process matched such previous growths well, so a QE in the region of a few percent was a reasonable expectation. Bi-alkali photocathodes are considerably more prone to contamination than Cs-Te photocathodes, so this cathode may have suffered a much higher level of QE degradation as a consequence of transportation to Daresbury, particularly if the levels of vibration during transit were high which would in turn increase the level of out-gassing in the transport vessel.

An experiment with the Cs-K-Sb cathode intended to recover lost QE was successful, in that we demonstrated that controlled heating to around 100 °C roughly doubled the QE. However we also found that the QE was not uniform across the surface of the cathode as the value was seen to vary significantly when the laser spot was moved on the cathode surface, confirming the suspicions of our colleagues at CERN. The results of the STM surface roughness measurements demonstrated a progressive increase in average roughness with increasing radial displacement from the centre of the photocathode, and it is reasonable to suggest that this increase in roughness is accompanied by a progressive decrease in QE, so appears consistent with the premise that QE decreases with radius.

8.3 Future work

It is pleasing to note that the project has demonstrated our ability to grow photocathodes at a central European laboratory, then transport them over several hundred miles

under UHV vacuum conditions to another laboratory whilst maintaining their photoemissivity to some extent. The experience has highlighted some improvements which we might make in the vacuum transportation and monitoring, and any further work should only be carried out once CERN has completed upgrades to the CLIC/CTF3 photocathode preparation facility control system.

We would ideally seek to ensure that any future work in this collaboration benefits from:

- Improvements in the preparation and mounting of the copper photocathode substrate pucks;
- Improvements in quality control during photocathode growth to increase the product consistency;
- QE measurements at CERN after growth;
- Improvements to the pumping arrangements and vacuum performance of the vacuum suitcase;
- The addition of some facility to monitor and record the pressure in the vacuum suitcase during transportation;
- Improvements in the vacuum of the Multiprobe sample loading interface;
- QE measurements at Daresbury as soon as possible following transportation.

9 Acknowledgements

The work documented in this report was carried out by Pavel Juarez–Lopez and Liam Soomary, both Ph.D. research students with the University of Liverpool and the Cockcroft Institute of Accelerator Science, supervised by Dr. Lee Jones (for ASTeC) and Prof. Carsten Welsch (for the University of Liverpool).

The work was partly–funded by the Mexican government through the *Consejo Nacional de Ciencia y Tecnologia* (https://www.conacyt.gob.mx/).

A Caesium work function and the concept of *Excess Energy* during photoemission.

Another approach to better understand the results presented in Section 5 is to consider the interplay between the work function for caesium and the photocathode illumination wavelength. As the work function is known, we can estimate the MTE based on the illumination wavelength and compare this with the experimental data taken.

Michaelson quotes a value of 2.14 eV for the caesium work function (ϕ) [Michaelson, 1977] and Cultrera suggested the following approximation relating the MTE to the excess energy in a photoemission event to a scaling factor [Cultrera et al., 2013]:

$$\text{MTE} \approx \frac{1}{3}(h\nu - \phi) \tag{2}$$

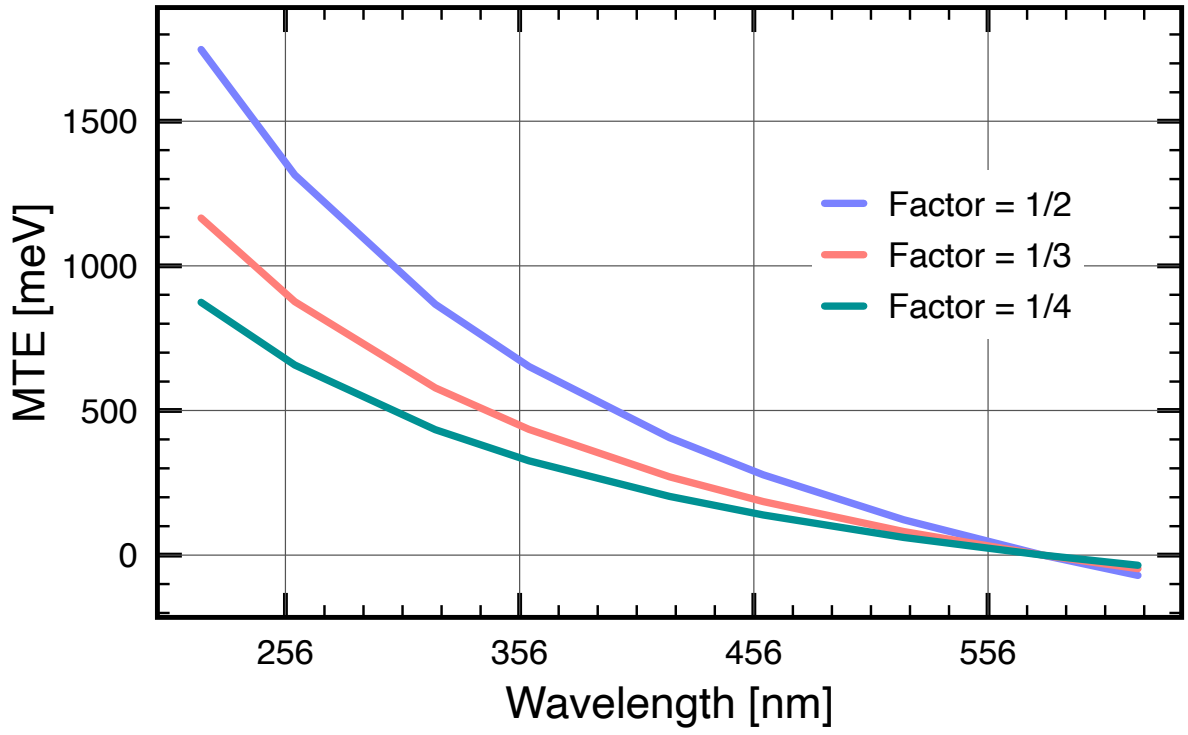

Figure 18: MTE approximation for photoemission from caesium based on excess energy.

Figure 18 shows MTE values calculated using equation 2 with a work function of 2.14 eV for caesium but using 3 different scaling factors. The purple line corresponds to a factor of $\frac{1}{2}$ and results in the highest MTE values at short wavelengths. The red line corresponds to a factor of $\frac{1}{3}$, as suggested by [Cultrera et al., 2013], and the green line corresponds to a factor of $\frac{1}{4}$.

As can be seen in Figure 18, the MTE approximated by equation 2 falls to zero at a wavelength of 579 nm, implying that the caesiated photocathode will only photoemit

at shorter wavelengths. In reality, the lower limit for MTE is governed by the photocathode temperature through the kT energy relationship, and as kT at room temperature is approximately 25 meV, the emission threshold will be moved to a slightly shorter wavelength.

However the MTE values approximated using equation 2 do not agree that well with those measured in the caesiation experiment, as can be seen in Table 5. There is an inconsistency as the MTE under illumination at 266 nm is reasonably well approximated using a scaling factor of $\frac{1}{4}$ while that at 532 nm is better approximated using a factor of $\frac{1}{2}$.

B STM line scan data for the P1 and P3 photocathodes

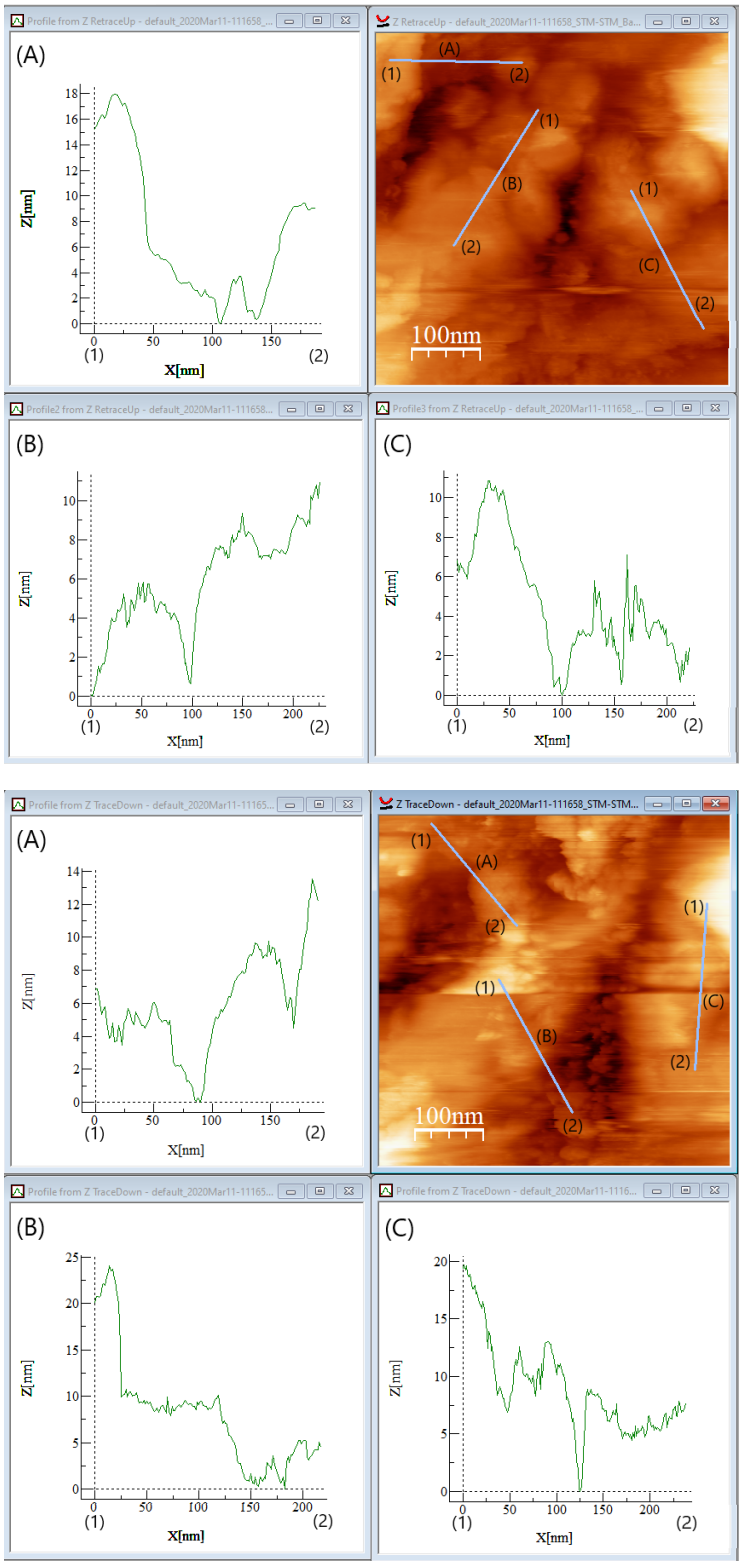

Figure 19: STM line profiles for the **P1 Cs–Te** at position 1 **(top)** and position 2 **(bottom)**.

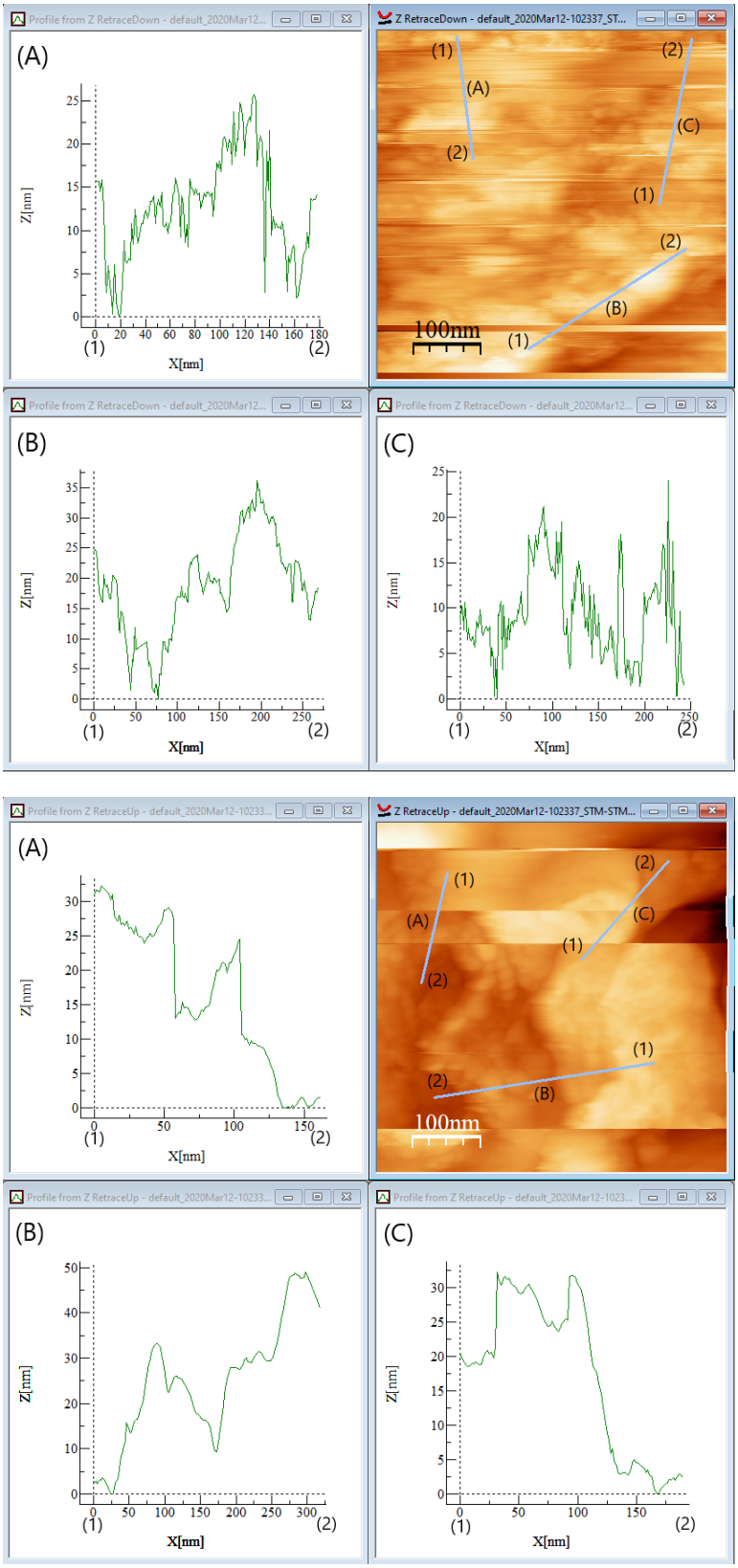

Figure 20: STM line profiles for **P1 Cs–Te** at position 3 **(top)** and position 4 **(bottom)**.

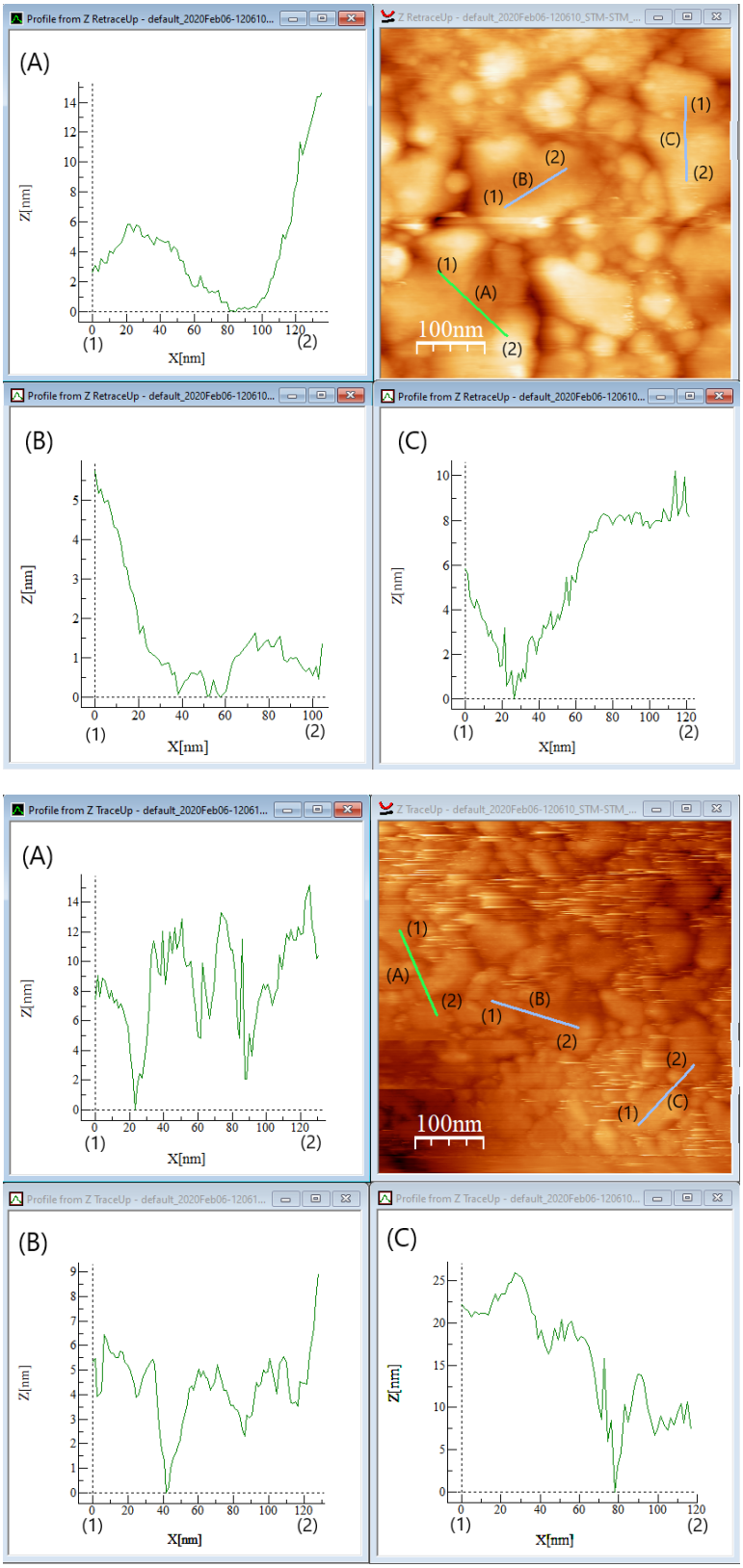

Figure 21: STM line profiles for **P3 Cs–K–Sb** at position 1 **(top)** and position 3 **(bottom)**.

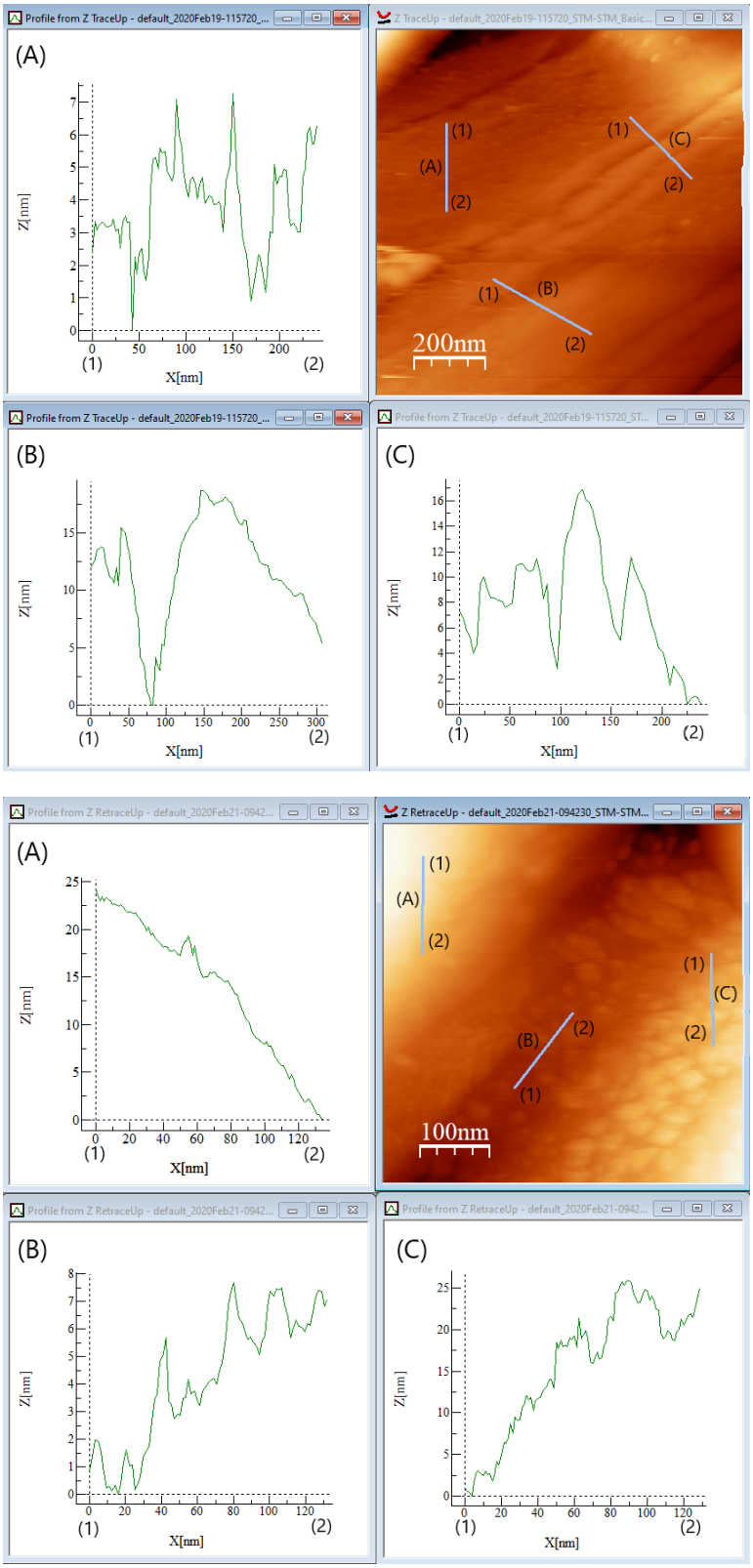

Figure 22: STM line profiles for **P3 Cs–K–Sb** at position 3 **(top)** and position 4 **(bottom)**.

References

Chevallay, E. et al. (2012). 'PHIN photo-injector as the CLIC drive beam source'. In: *Journal of Physics: Conference Series* 347, p. 012036. DOI: https://doi.org/10.1088/1742-6596/347/1/012036.

Cultrera, L. et al. (2013). 'Growth and characterization of rugged sodium potassium antimonide photocathodes for high brilliance photoinjector'. In: *Appl. Phys. Lett.* 103. DOI: https://doi.org/10.1063/1.4820132.

Gaowei, M. et al. (2019). 'Codeposition of ultrasmooth and high quantum efficiency cesium telluride photocathodes'. In: *Phys. Rev. Accel. Beams* 22 (7), p. 073401. DOI: https://doi.org/10.1103/PhysRevAccelBeams.22.073401.

Jones, L. B. et al. (2017). 'Evolution of the transverse and longitudinal energy distributions of electrons emitted from a GaAsP photocathode as a function of its degradation state'. In: *Journal of Applied Physics* 121.22, p. 225703. DOI: https://doi.org/10.1063/1.4984603.

Jones, L.B. et al. (2013). 'The Commissioning of Tess: An Experimental Facility for Measuring the Electron Energy Distribution From Photocathodes'. In: *FEL 2013* TUPSO33, p. 290.

Michaelson, H.B. (1977). 'The work function of the elements and its periodicity'. In: *J. Appl. Phys.* 48. DOI: https://doi.org/10.1063/1.323539.

Noakes, T.C.Q. et al. (2014). *Commissioning of the SAPI for Operation with Metal Photocathodes*. Tech. rep. STFC.

Panuganti, H. et al. (2020). 'Synthesis, surface chemical analysis, lifetime studies and degradation mechanisms of Cs-K-Sb photocathodes [Submitted]'. In: - -, pp. –.

Yeh, J.J. and I. Lindau (1985). 'Atomic subshell photoionization cross sections and asymmetry parameters: $1 < Z < 103$'. In: *Atomic Data and Nuclear Data Tables* 32.1, pp. 1 –155. ISSN: 0092-640X. DOI: https://doi.org/10.1016/0092-640X(85)90016-6.